

独立成分分析を用いた重力波抽出方法の提案

[arXiv:2503.14179](https://arxiv.org/abs/2503.14179)

Gravitational-wave Extraction using Independent Component Analysis

下村りか, 田部優一, 真貝寿明 (大阪工大情報科学部)

Rika Shimomura, Yuuichi Tabe, Hisaaki Shinkai (OIT)

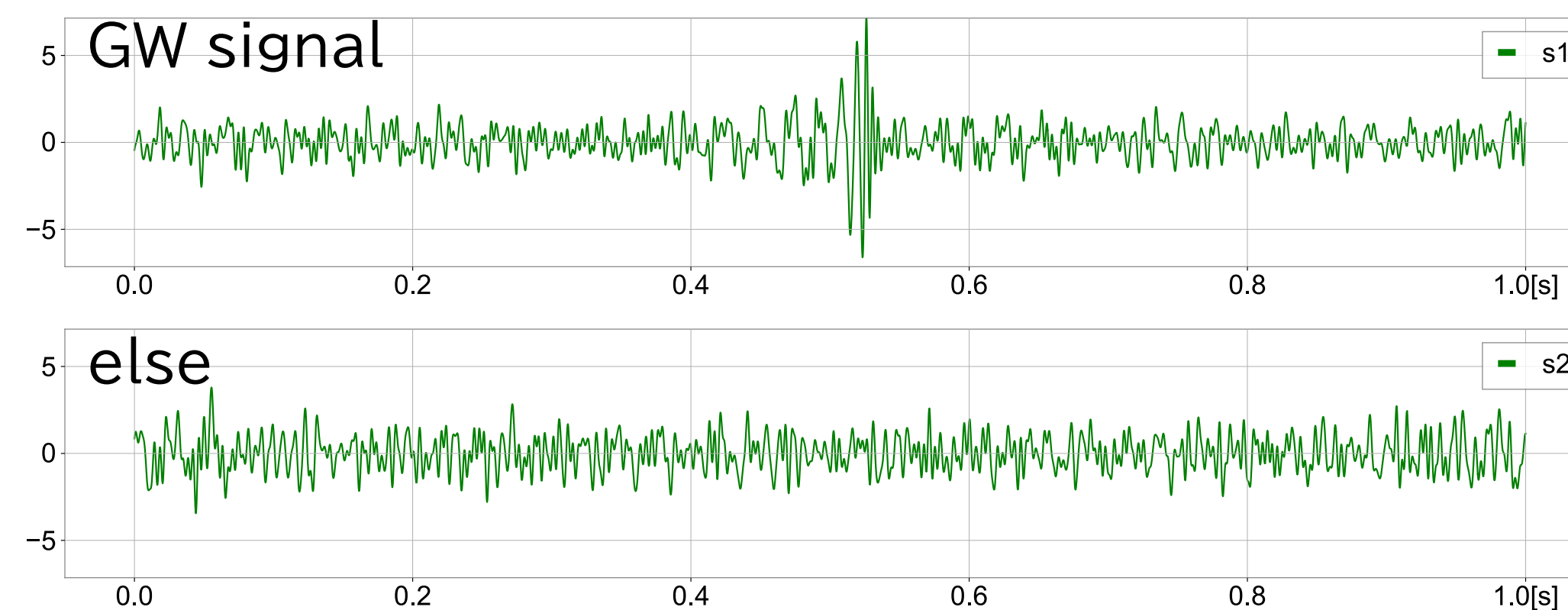
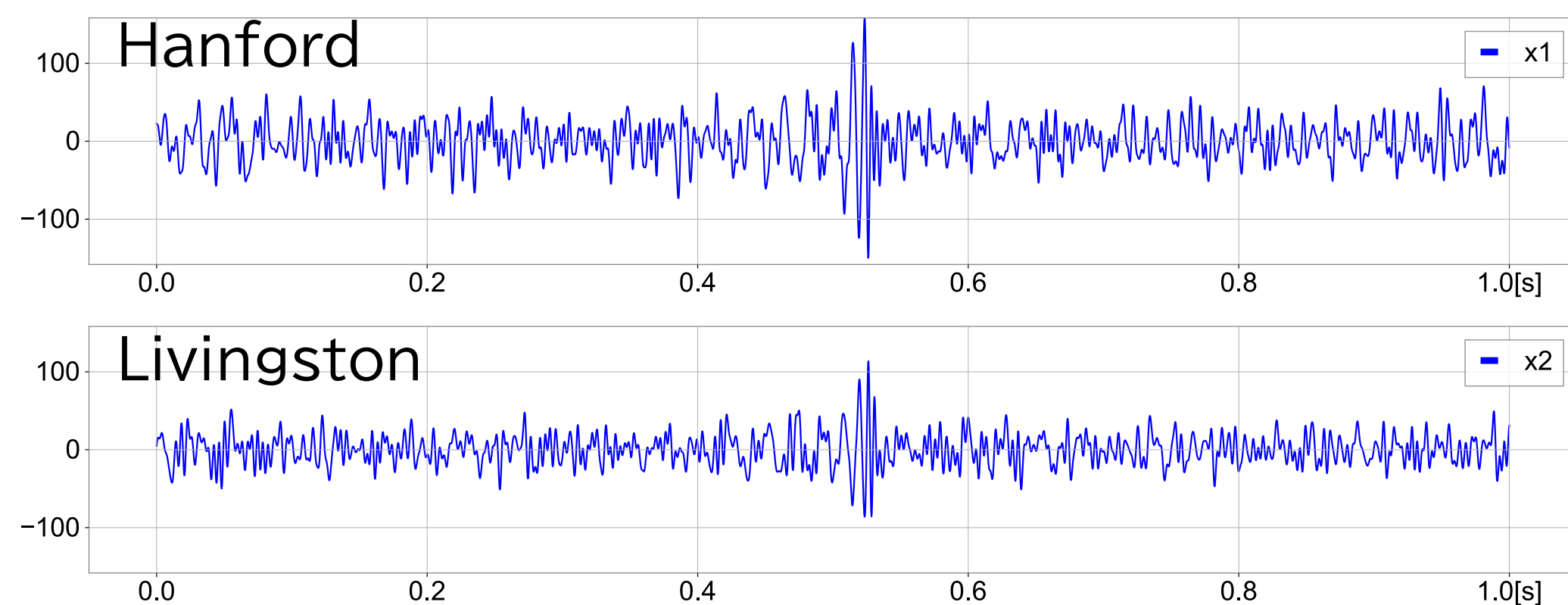
目的

- テンプレートを用いずに、重力波の波形を取り出す新たな手法を提案する
 - 一般相対性理論の検証
 - 未知の重力波の発見

結論

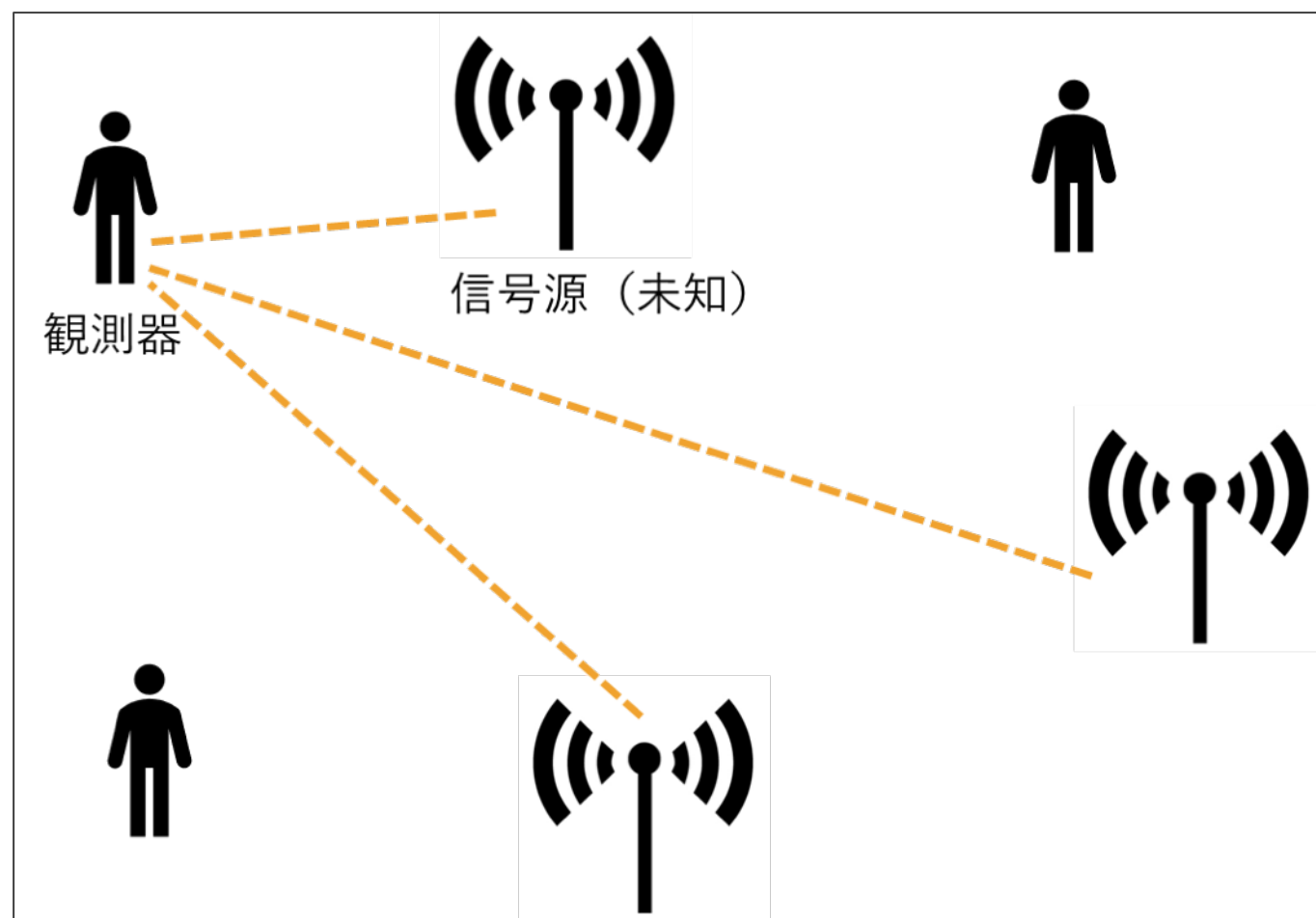
- Injection testにより、干渉計の実ノイズでも、 $\text{SNR} > 15$ で有効
- O3までの実イベント10例以上に応用
 - 波形を抽出でき、 $M_c(1+z)$ も GWTC3と無矛盾
 - 干渉計への重力波到着時刻の誤差を小さくできる例あり

GW150914



探すべき成分が統計的に独立であり、非ガウスの場合、多変量のデータから隠された因子や成分を見つけ出す手法

Blind Source Separation(ブラインド信号源分離)



3つの観測信号から、信号源の信号3つを推定する

$$\mathbf{x}(t) = \mathbf{A}\mathbf{s}(t)$$

観測データ 係数行列 信号源

$$\tilde{\mathbf{s}}(t) = \mathbf{W}\mathbf{x}(t)$$

推定された信号 観測データ

この行列を求めたい!

統計的に独立 非ガウスの信号を取り出す
 ... ガウシアンから離れている信号を探す

ホワイトニングしたデータ列 $\mathbf{z}(t)$ にして、

$$s_i(t) = \mathbf{w}_i^T \mathbf{V}\mathbf{x}(t) \equiv \mathbf{w}_i^T \mathbf{z}(t)$$

尖度が最大となるような変換行列 \mathbf{W} を求める

$$\text{kurt}(\mathbf{w}^T \mathbf{z}) = E[(\mathbf{w}^T \mathbf{z})^4] - 3\{E[(\mathbf{w}^T \mathbf{z})^2]\}^2$$

収束するまで繰り返しながら

$$\frac{\partial}{\partial \mathbf{w}_i} |\text{kurt}(\mathbf{w}_i^T \mathbf{z})| = \begin{pmatrix} E[4(\mathbf{w}_i^T \mathbf{z})^3 z_1] \\ E[4(\mathbf{w}_i^T \mathbf{z})^3 z_2] \\ \vdots \end{pmatrix} - 12\|\mathbf{w}_i\|^2 \begin{pmatrix} w_{11} \\ w_{12} \\ \vdots \end{pmatrix}$$

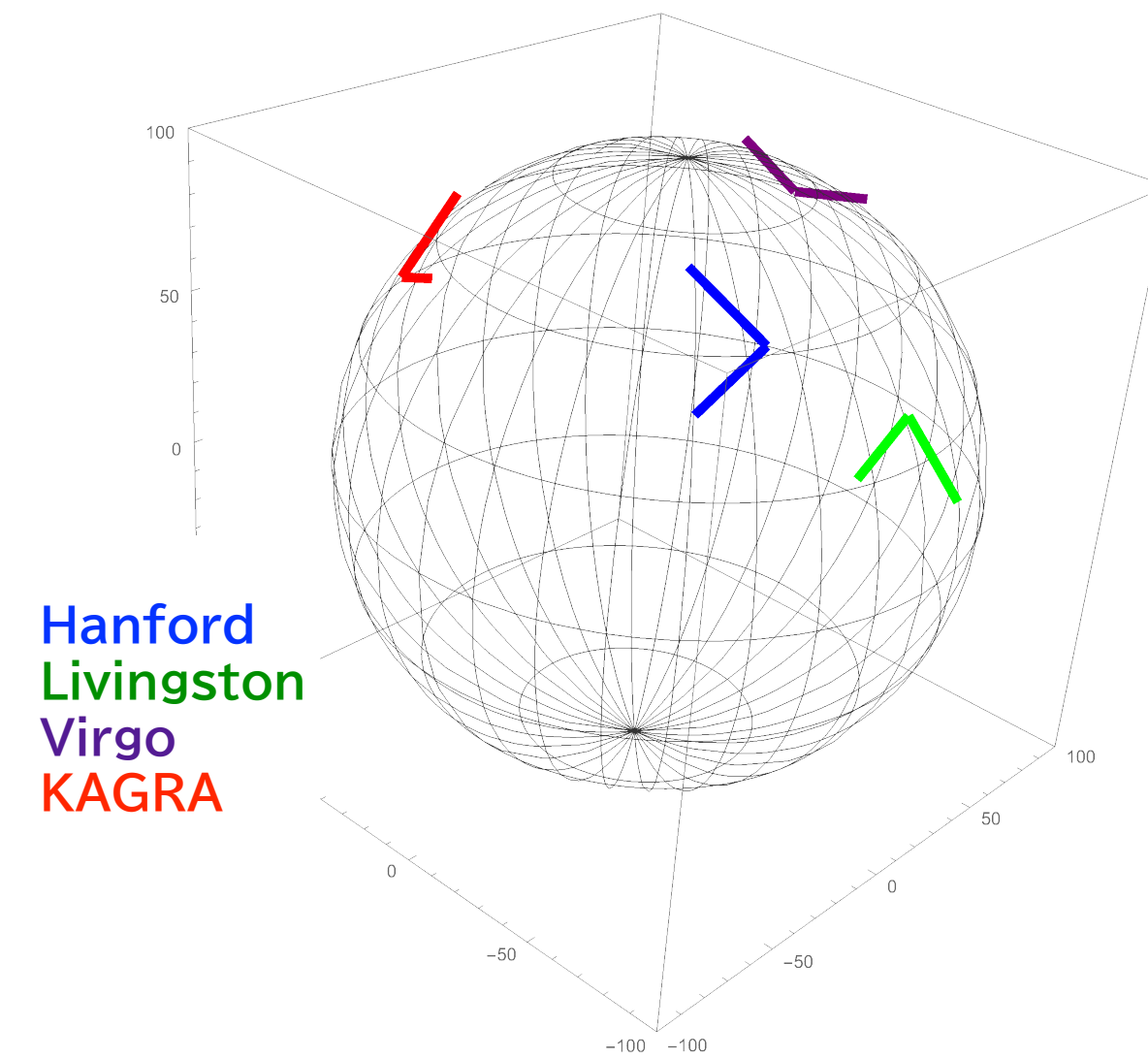
実際には 尖度は、外れ値に引きずられることが多いので、g関数法と呼ばれる $\mathbf{w}_p = E[\mathbf{z}g(\mathbf{w}_p^T \mathbf{z})] - E[g'(\mathbf{w}_p^T \mathbf{z})]\mathbf{w}_p$

where $g(y) = \tanh y$. とする手法を用いる (FastICA法の1つ).

独立成分分析の重力波データ解析への応用

これまでの重力波に関連するreferences

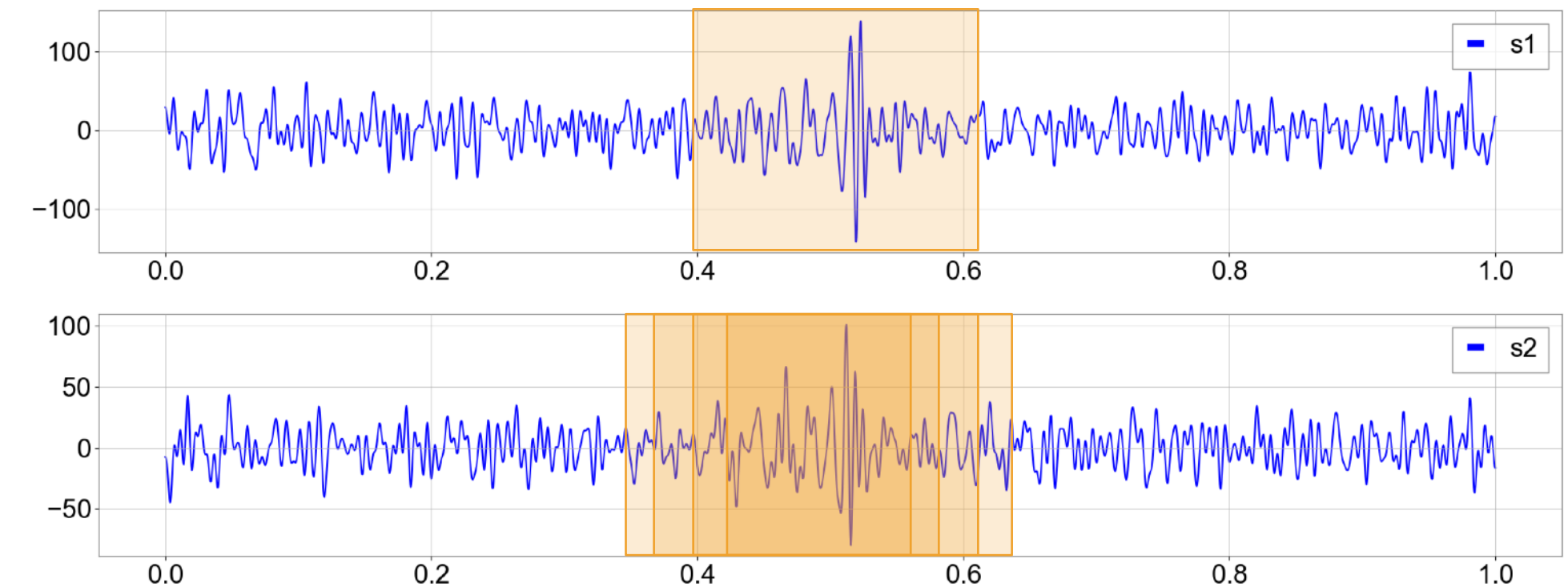
- [1] R. De Rosa, et al., CQG 29, 215008 (2012)
Matched-Filter解析の前処理にICAを用いることで、重力波の検出効率を高められる可能性を干渉計のmock dataで示す
- [2] S. Morisaki, J. Yokoyama, K. Eda, Y. Itoh, J.Comp. Phys. 300, 275 (2016)
非ガウス性ノイズ除去への応用可能性を指摘
- [3] KAGRA Collaboration, CQG 40, 085015 (2023)
iKAGRA観測時(2020)の実データを用いて、地震計などの物理環境チャンネル信号を例に、ICAによるノイズ除去の実例を示す



➤ 実際の干渉計のデータに対して重力波の抽出を試みた研究はない

論点

実際の干渉計データから重力波を取り出すことができるのか
どこまでのSNRの波を取り出せるのか



特別な工夫 干渉計データの時刻をずらしながら、最もよく信号が抽出できる状況を探す

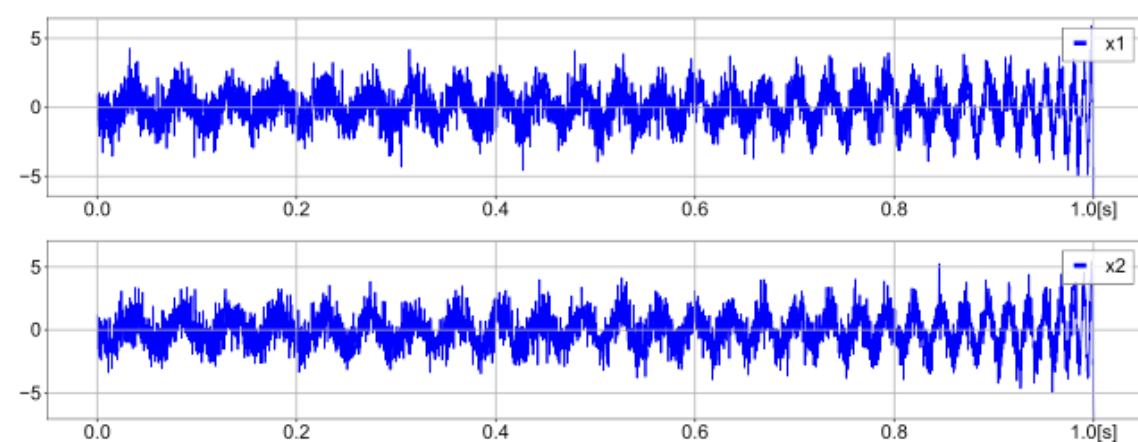
テスト計算1: 2つの異なるガウス分布 + inspiral-wave injection

$$\text{Model 1: } \begin{cases} x_1(t) = n_{1G}(t) + h_{\text{insp}}(t; t_c, M_c), \\ x_2(t) = n_{2G}(t) + h_{\text{insp}}(t; t_c, M_c). \end{cases}$$

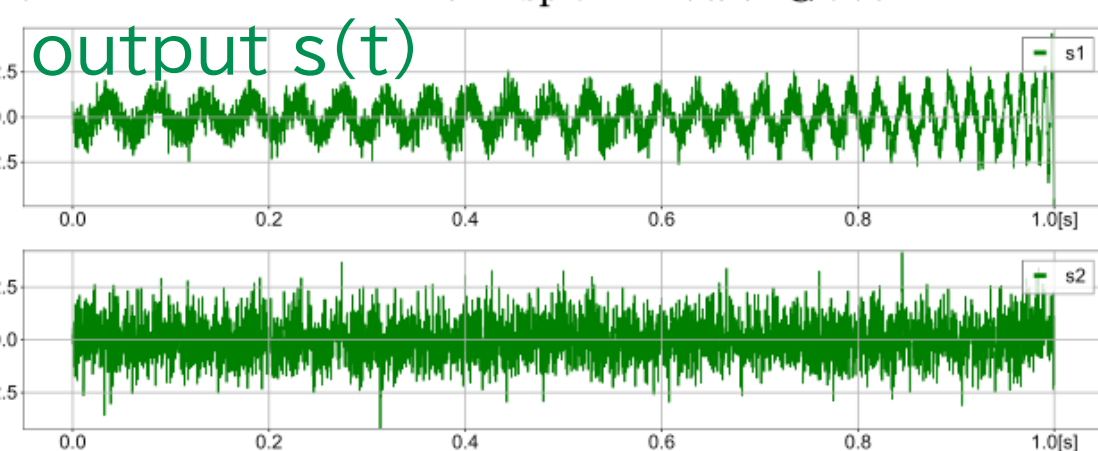
➡ 振幅が小さいと、ガウスノイズからの分離も困難

injection波の振幅 = 5 x ノイズ

input $x(t)$

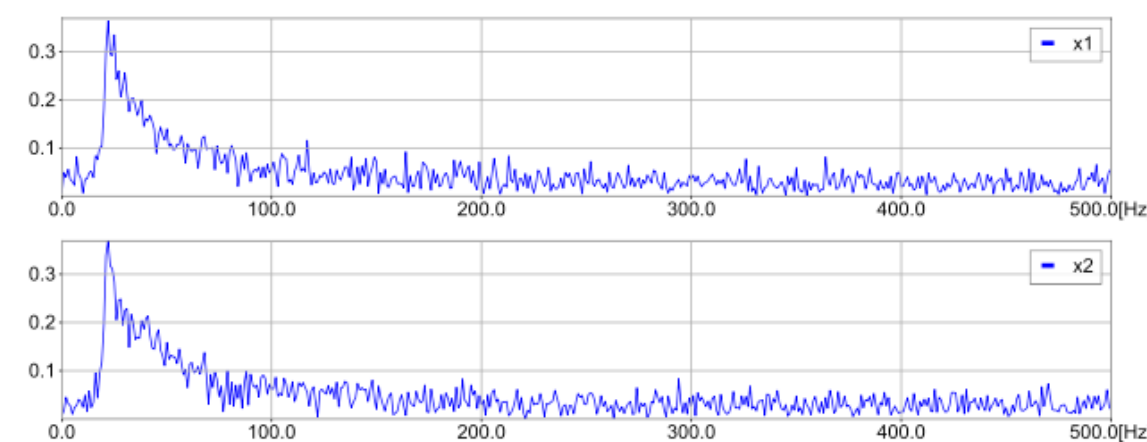


(a1) Input signals with $|h_{\text{insp}}(t=1)|/|\overline{n_G(t)}| = 5.0$.

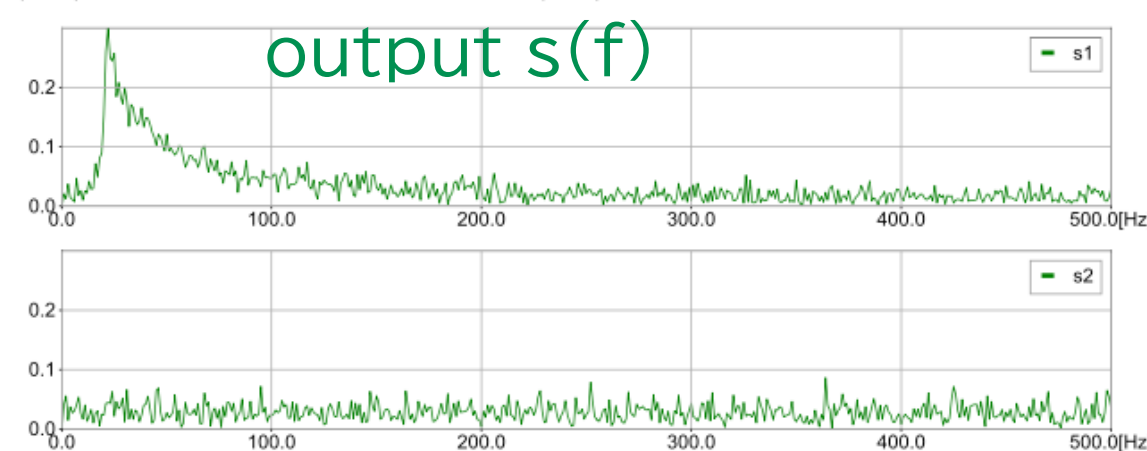


(a3) Output of ICA for (a1).

input $x(f)$

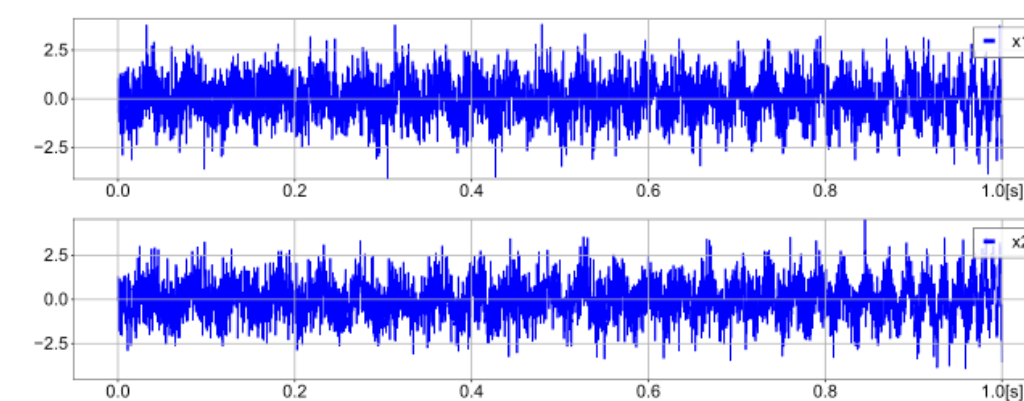


(a2) Fourier spectrum of (a1).

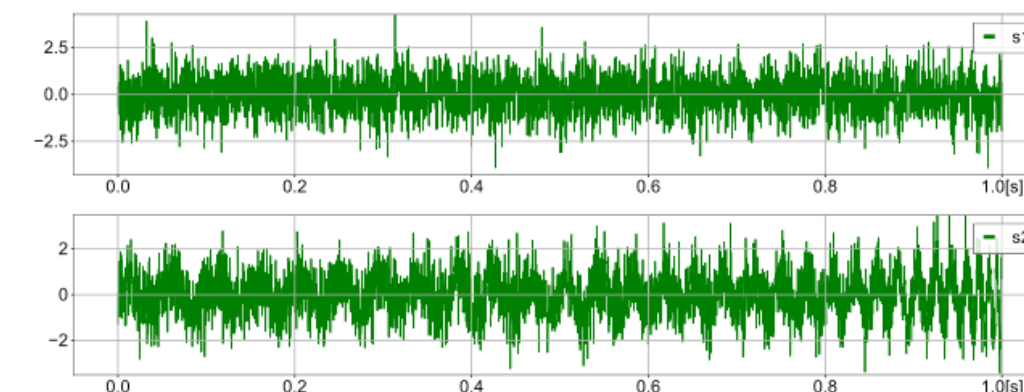


(a4) Fourier spectrum of (a3).

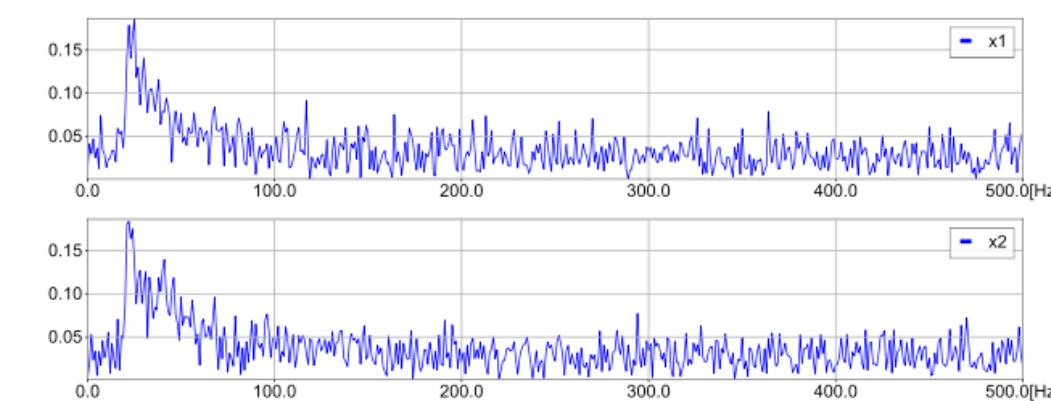
injection波の振幅 = 2.5 x ノイズ



(b1) Input signals with $|h_{\text{insp}}(t=1)|/|\overline{n_G(t)}| = 2.5$.



(b3) Output of ICA for (b1).

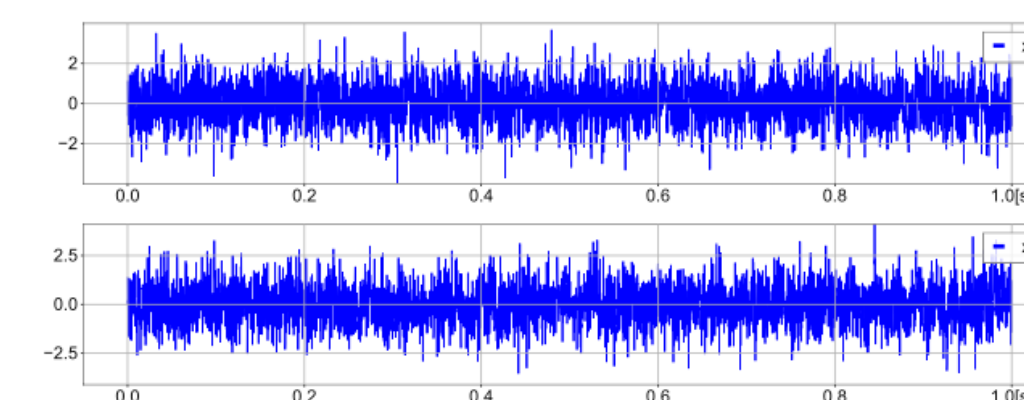


(b2) Fourier spectrum of (b1).

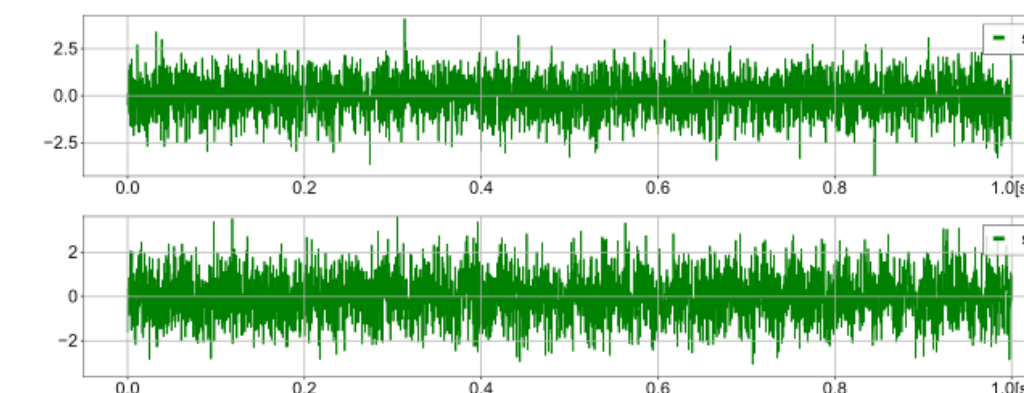


(b4) Fourier spectrum of (b3).

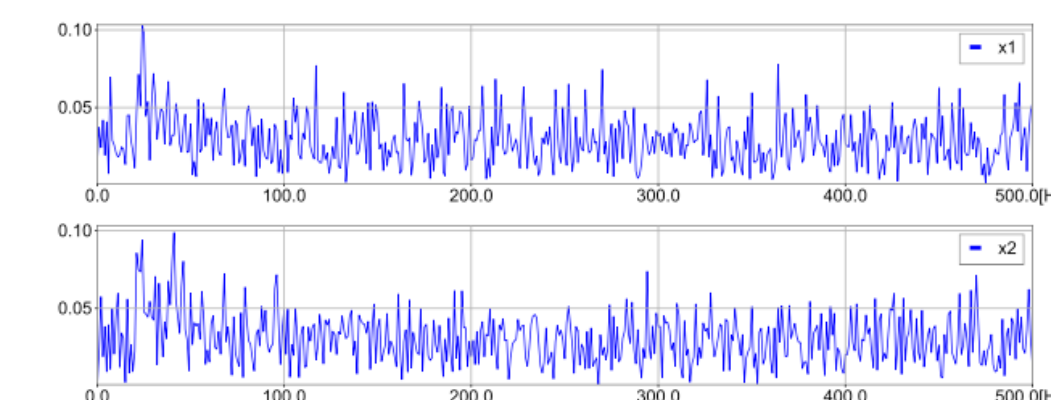
injection波の振幅 = 1.0 x ノイズ



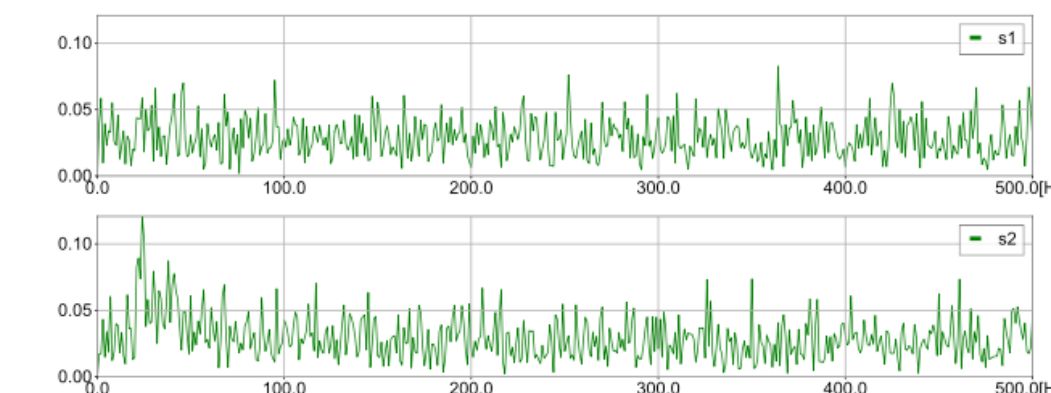
(c1) Input signals with $|h_{\text{insp}}(t=1)|/|\overline{n_G(t)}| = 1.0$.



(c3) Output of ICA for (c1).



(c2) Fourier spectrum of (c1).



(c4) Fourier spectrum of (c3).

テスト計算2: Hanford/Livingston実ノイズ+三角関数injection

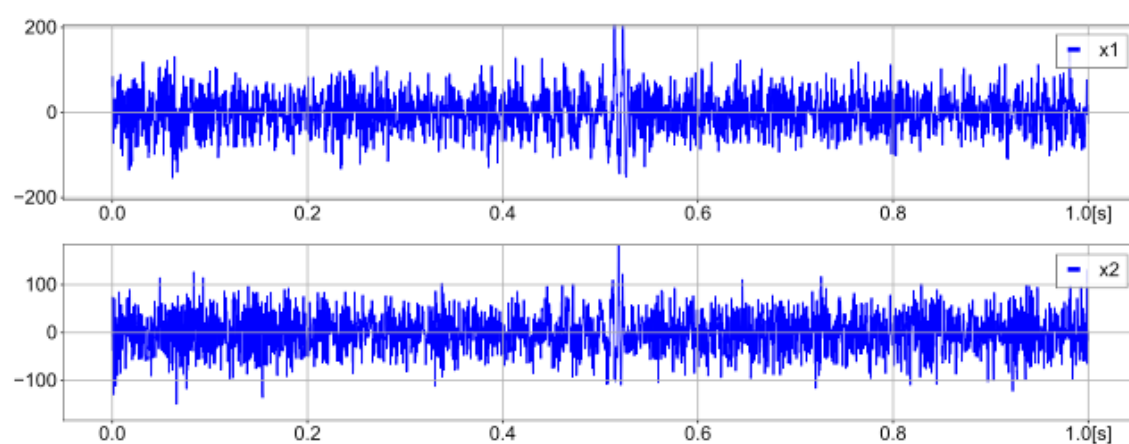
$$\text{Model 2 : } \begin{cases} x_1(t) = n_H(t) + \sin(2\pi ft), \\ x_2(t) = n_L(t) + \sin(2\pi ft) \end{cases}$$

GW150914前後のHanford/Livingstonのデータに,
f=213Hzの波をinject

➡ SNR > 10 なら分離したものが認識できる

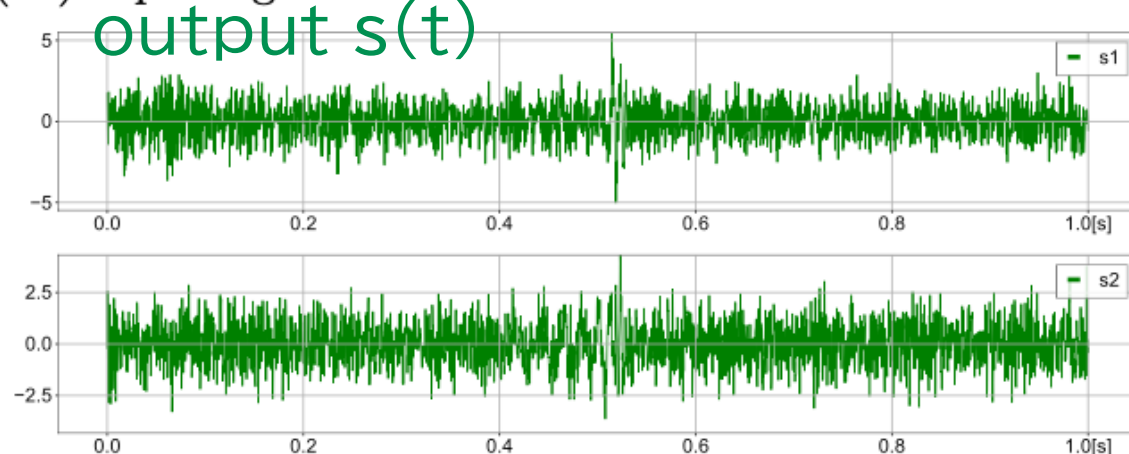
injection波のSNR = 20

input x(t)



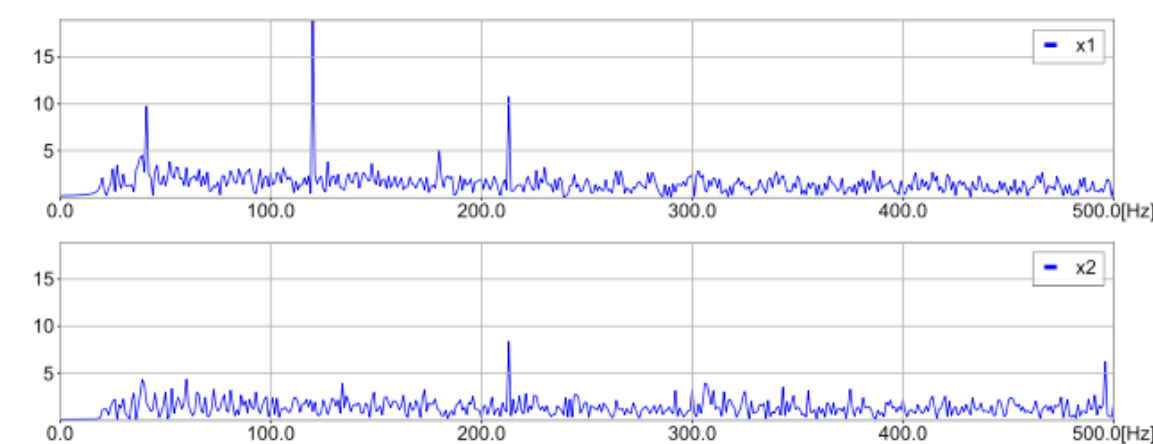
(a1) Input signals of SNR 20.

output s(t)



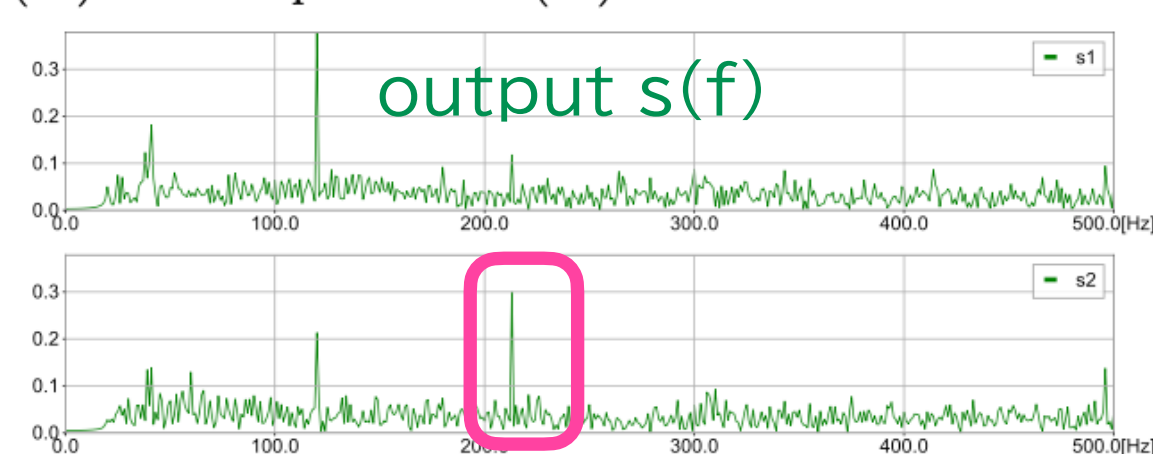
(a3) Output of ICA for (a1).

input x(f)



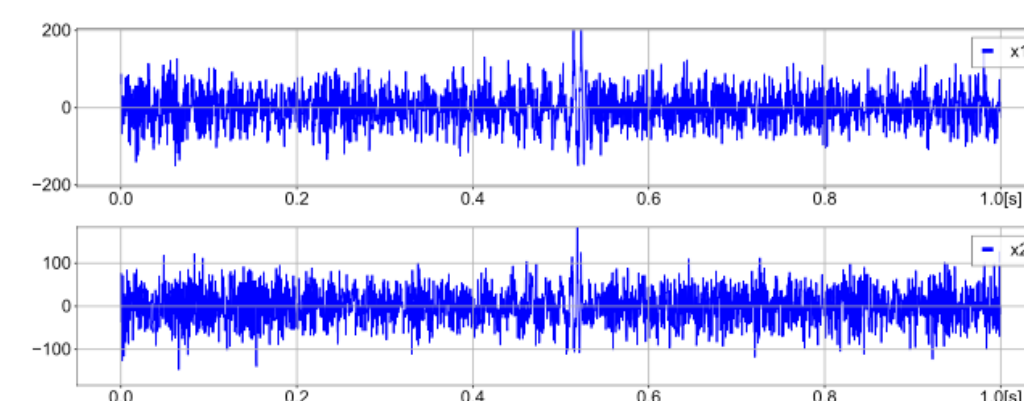
(a2) Fourier spectrum of (a1).

output s(f)

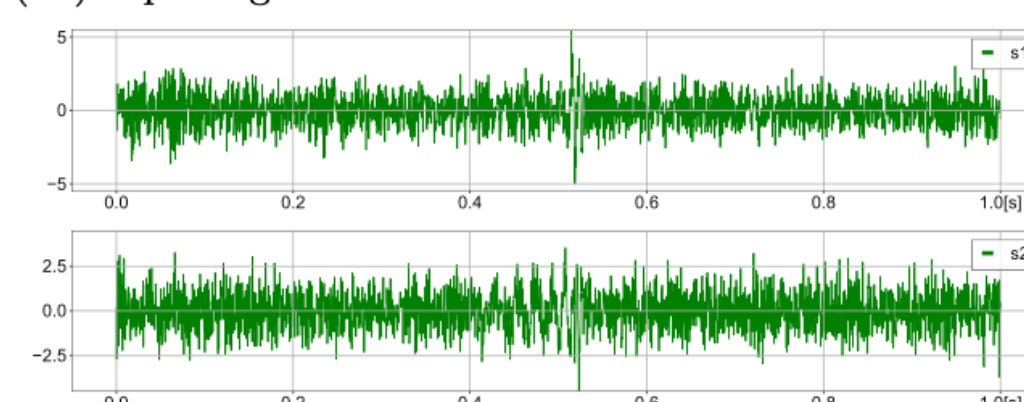


(a4) Fourier spectrum of (a3).

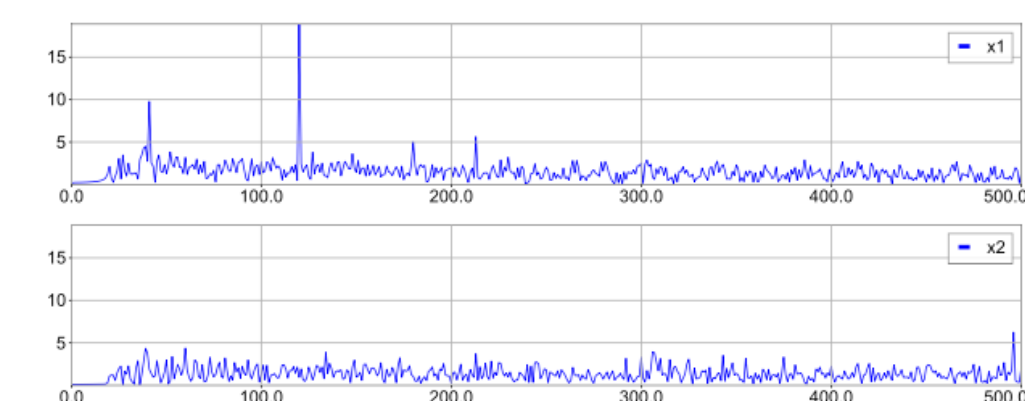
injection波のSNR = 10



(b1) Input signals of SNR 10.



(b3) Output of ICA for (b1).

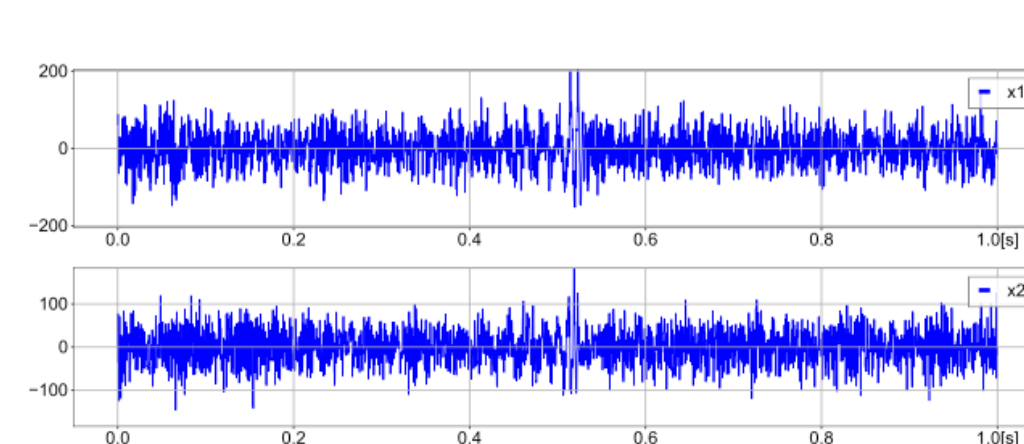


(b2) Fourier spectrum of (b1).

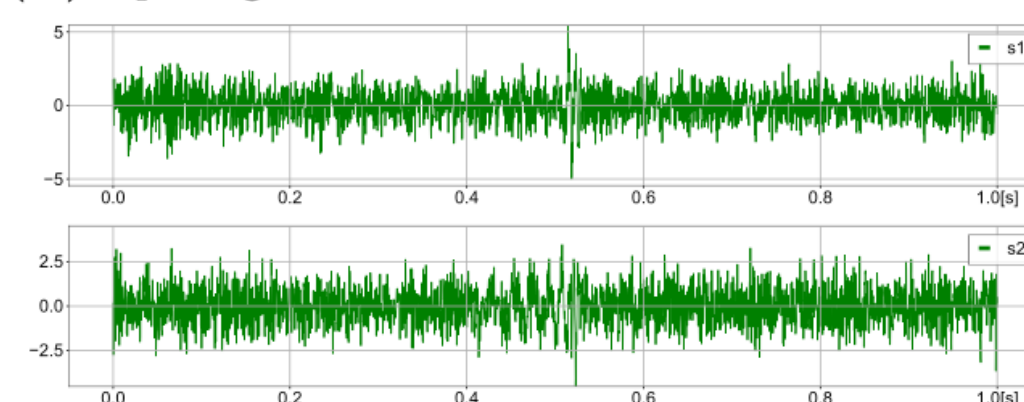


(b4) Fourier spectrum of (b3).

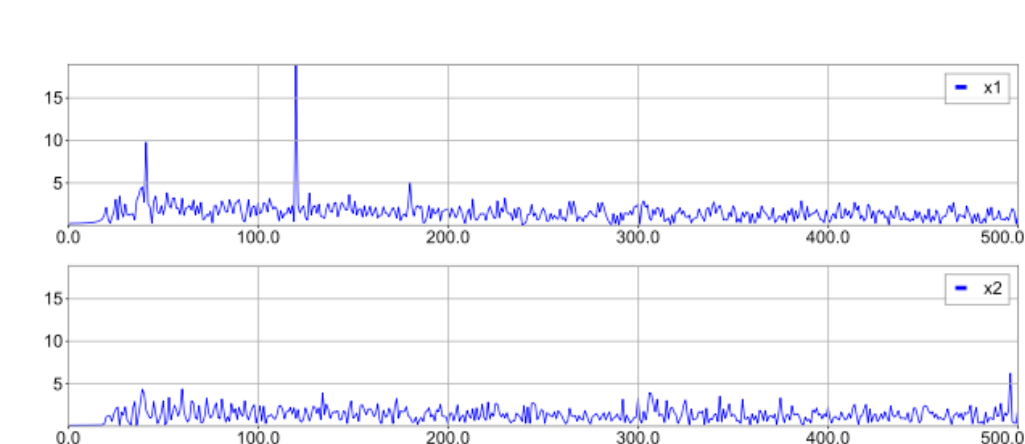
injection波のSNR = 5



(c1) Input signals of SNR 5.



(c3) Output of ICA for (c1).



(c2) Fourier spectrum of (c1).



(c4) Fourier spectrum of (c3).

テスト計算3: Hanford/Livingston実ノイズ+inspiral-wave injection

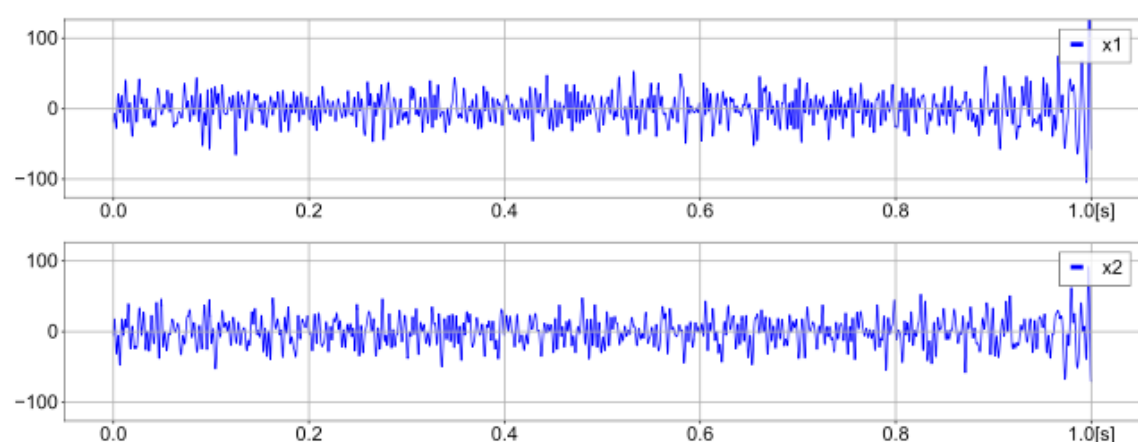
$$\text{Model 3 : } \begin{cases} s_1(t) = n_H(t) + h_{\text{insp}}(t; t_0, M_c), \\ s_2(t) = n_L(t) + h_{\text{insp}}(t; t_0, M_c). \end{cases}$$

GW150914前後のHanford/Livingstonのデータに,
inspiral 波をinject

➡ SNR > 15 なら分離したものが認識できる

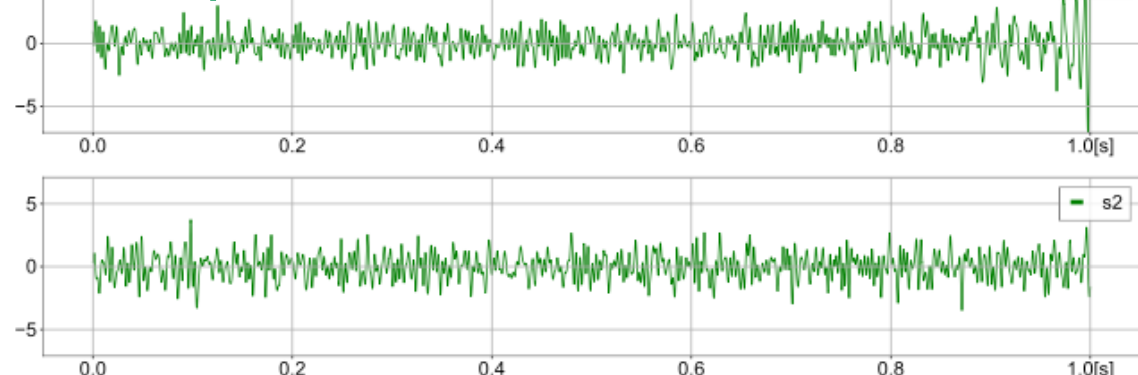
injection波のSNR = 20.9

input $x(t)$



(a1) Input signals of SNR 20.9.

output $s(t)$



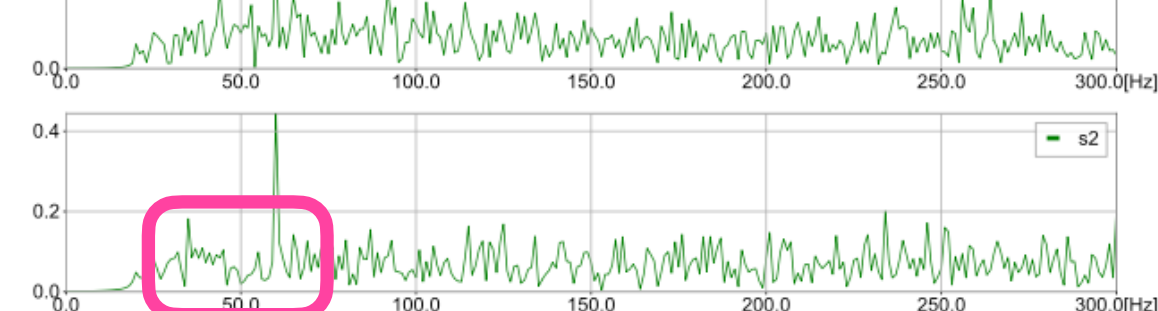
(a3) Output of ICA for (a1).

input $x(f)$



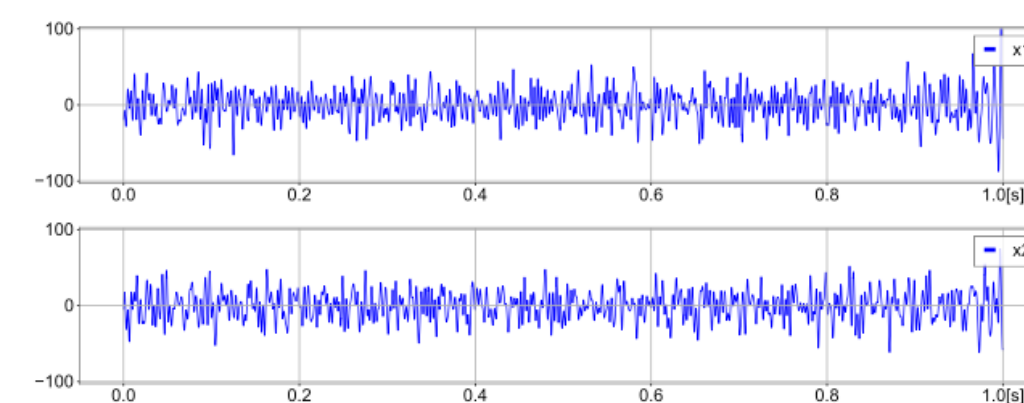
(a2) Fourier spectrum of (a1).

output $s(f)$

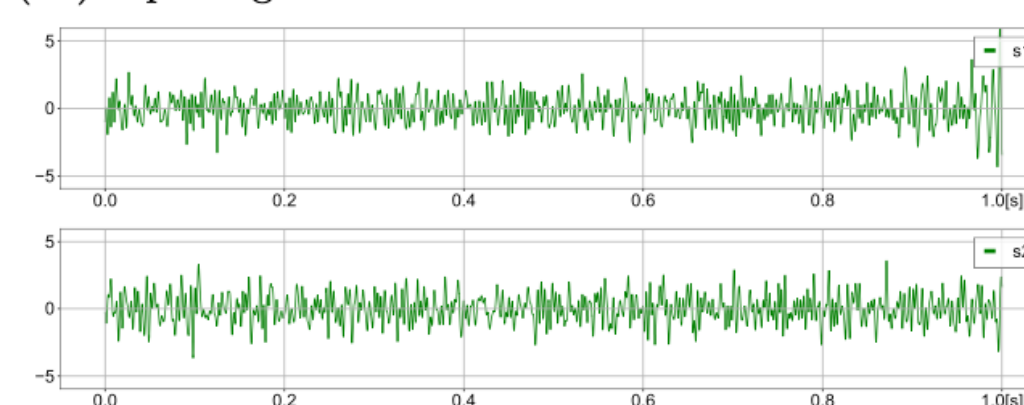


(a4) Fourier spectrum of (a3).

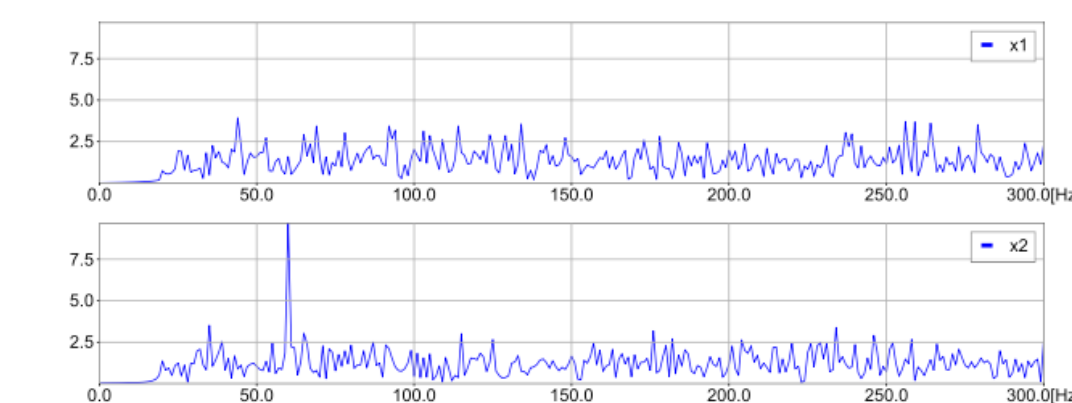
injection波のSNR = 16.8



(b1) Input signals of SNR 16.8.



(b3) Output of ICA for (b1).

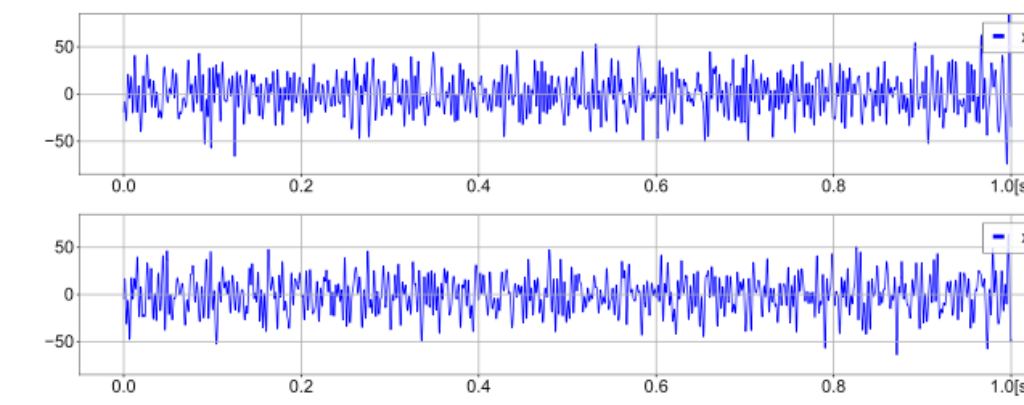


(b2) Fourier spectrum of (b1).

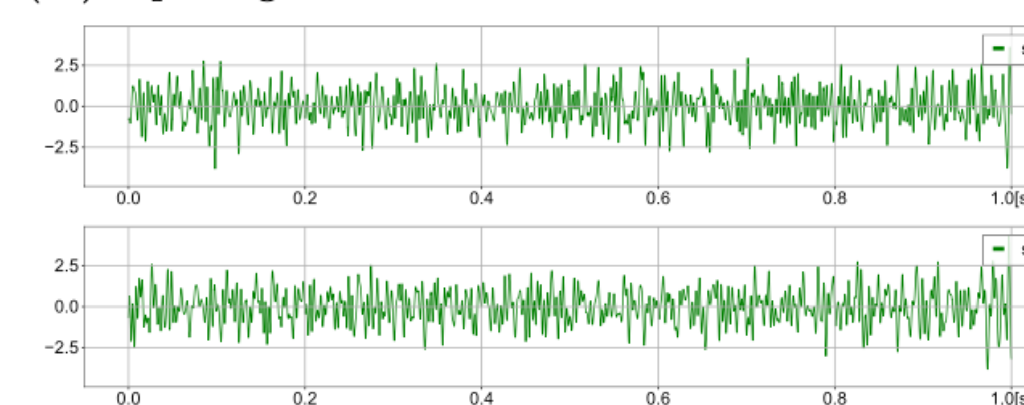


(b4) Fourier spectrum of (b3).

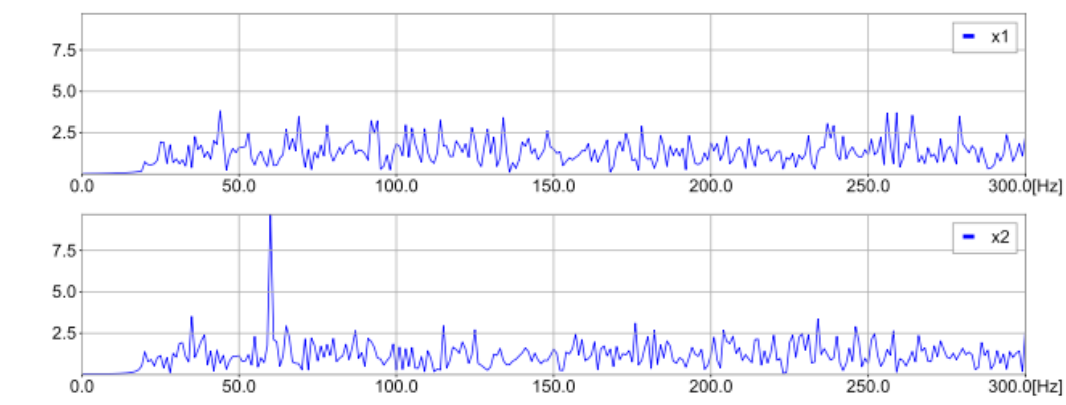
injection波のSNR = 10.5



(c1) Input signals of SNR 10.5.



(c3) Output of ICA for (c1).



(c2) Fourier spectrum of (c1)



(c4) Fourier spectrum of (c3).

実データへの応用: GW150914

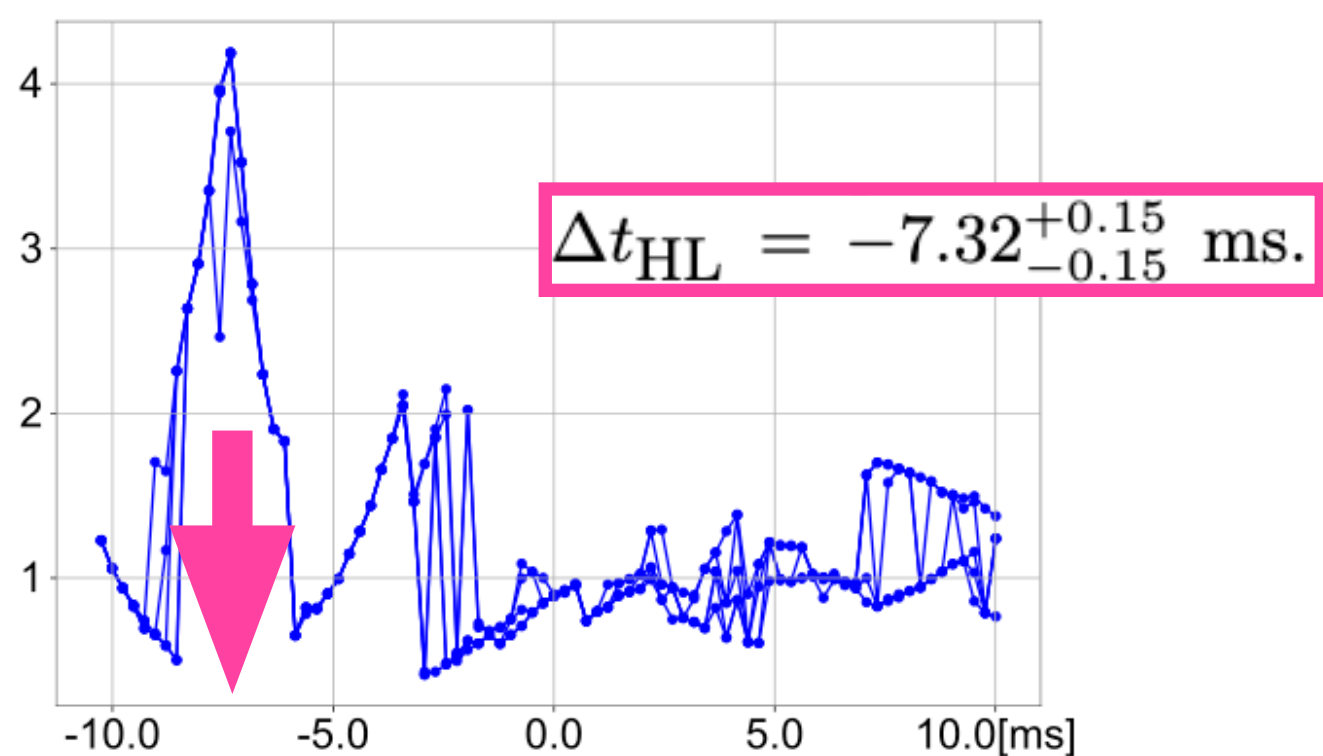
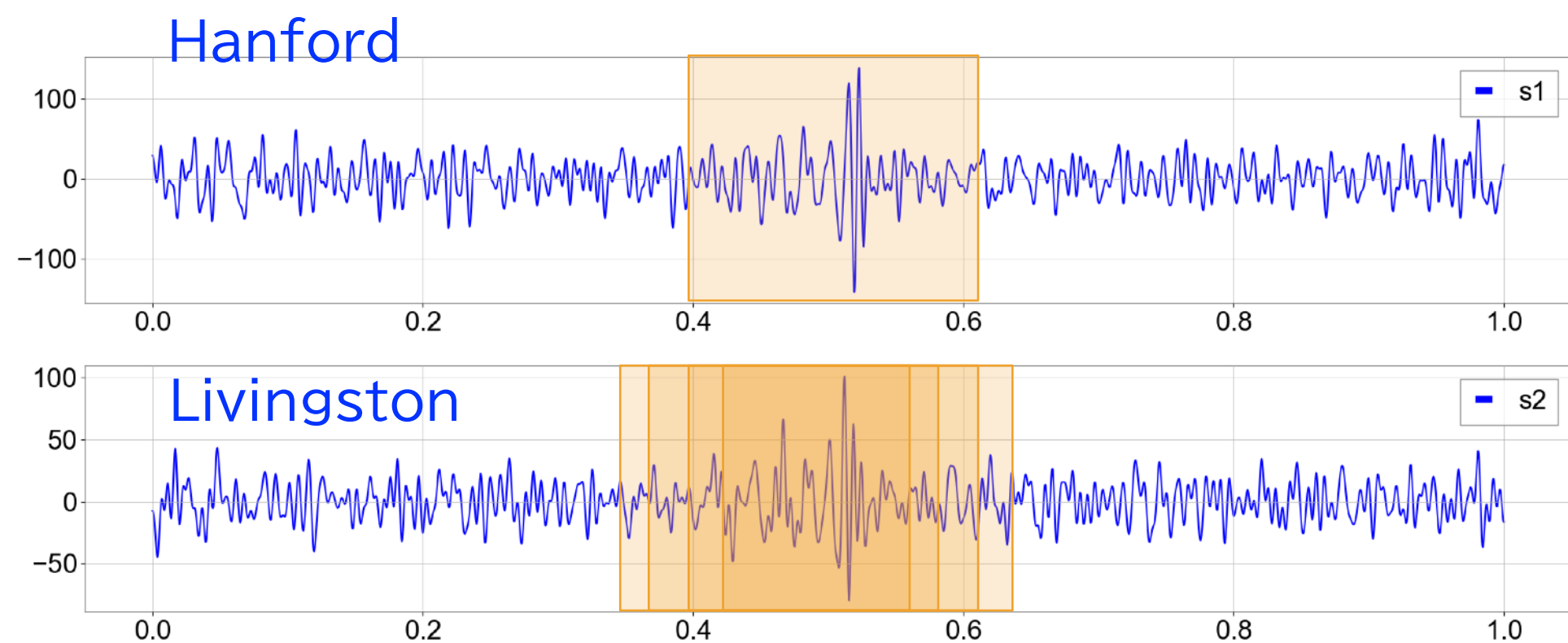
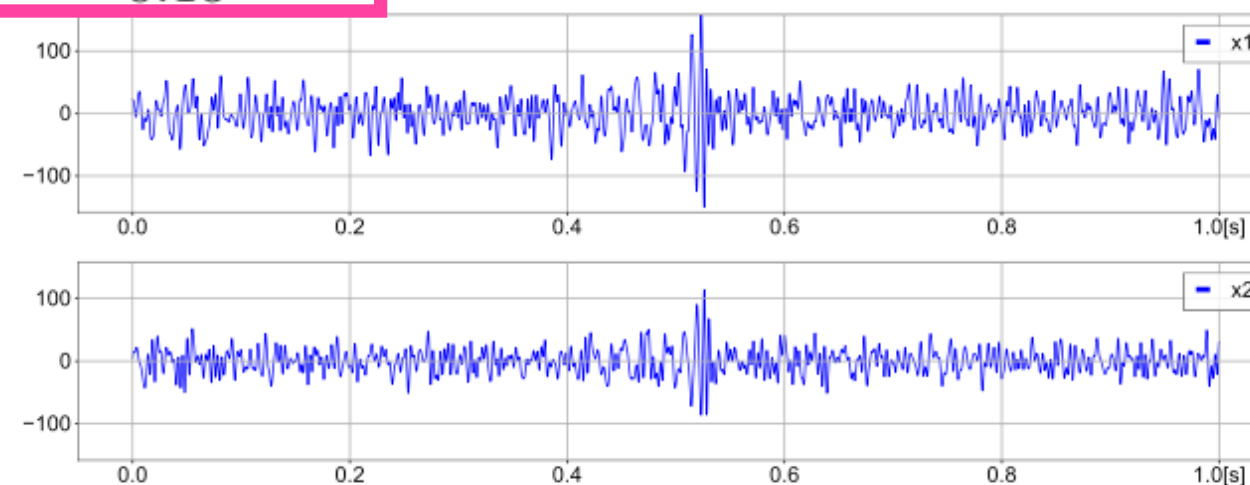


FIG. 5. The strength of the extracted signal, \mathcal{A} [eq. (10)] as a function of Δt_{HL} for the case of GW150914. Five trials of different initial weight matrix are plotted at each Δt_{HL} . We see the maximum is at $\Delta t_{\text{HL}} = -7.32^{+0.15}_{-0.15}$ ms. Note that LIGO-Virgo paper [1] shows $\Delta t_{\text{HL}} = 6.9^{+0.5}_{-0.4}$ ms.

$$\Delta t_{\text{HL}} = -6.9^{+0.5}_{-0.4} \text{ ms}$$

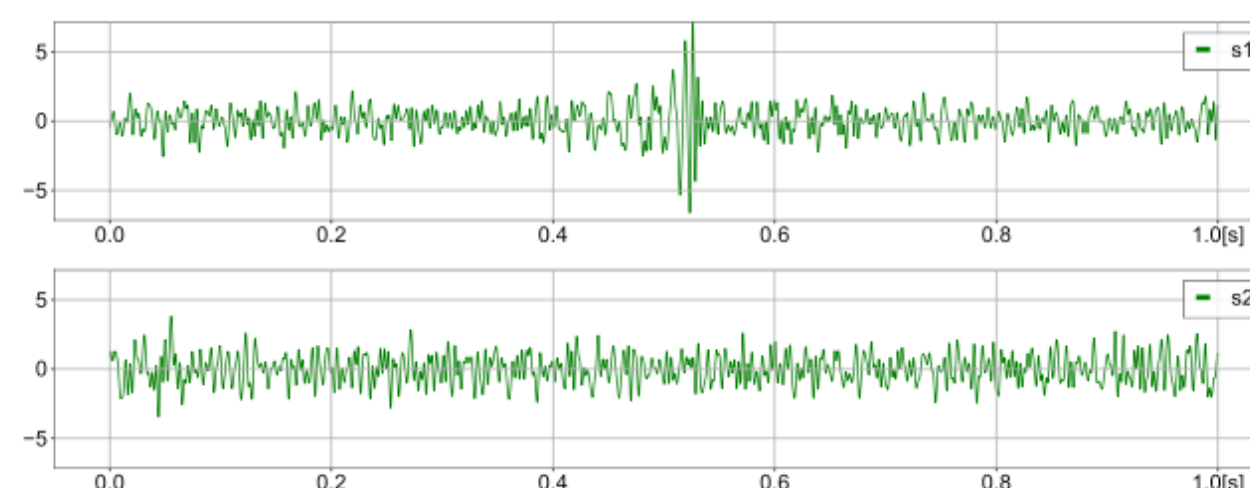
$$\Delta t_{\text{HL}} = -7.32^{+0.15}_{-0.15} \text{ ms.}$$

input $x(t)$

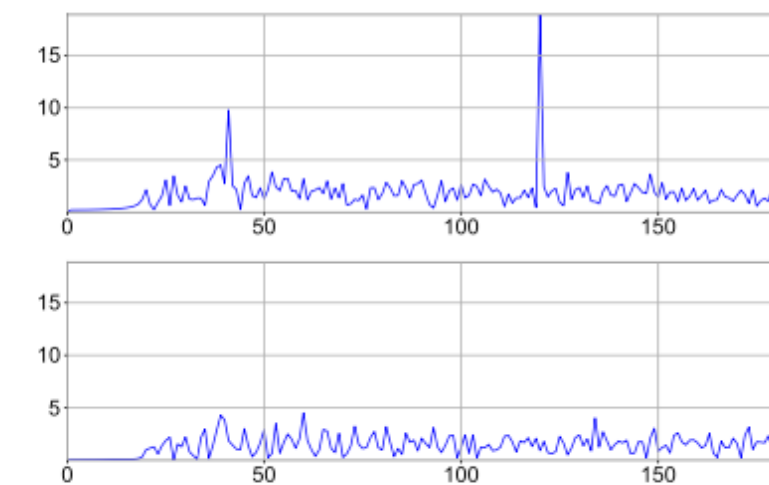


(a) Input signals with $\Delta t_{\text{HL}} = -7.32$ ms. The data x_1 and x_2 are of Hanford and Livingston data, respectively.

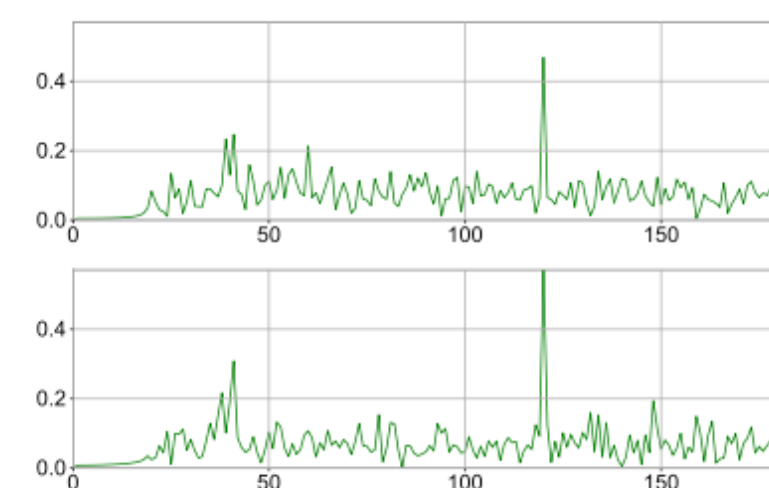
output $s(t)$



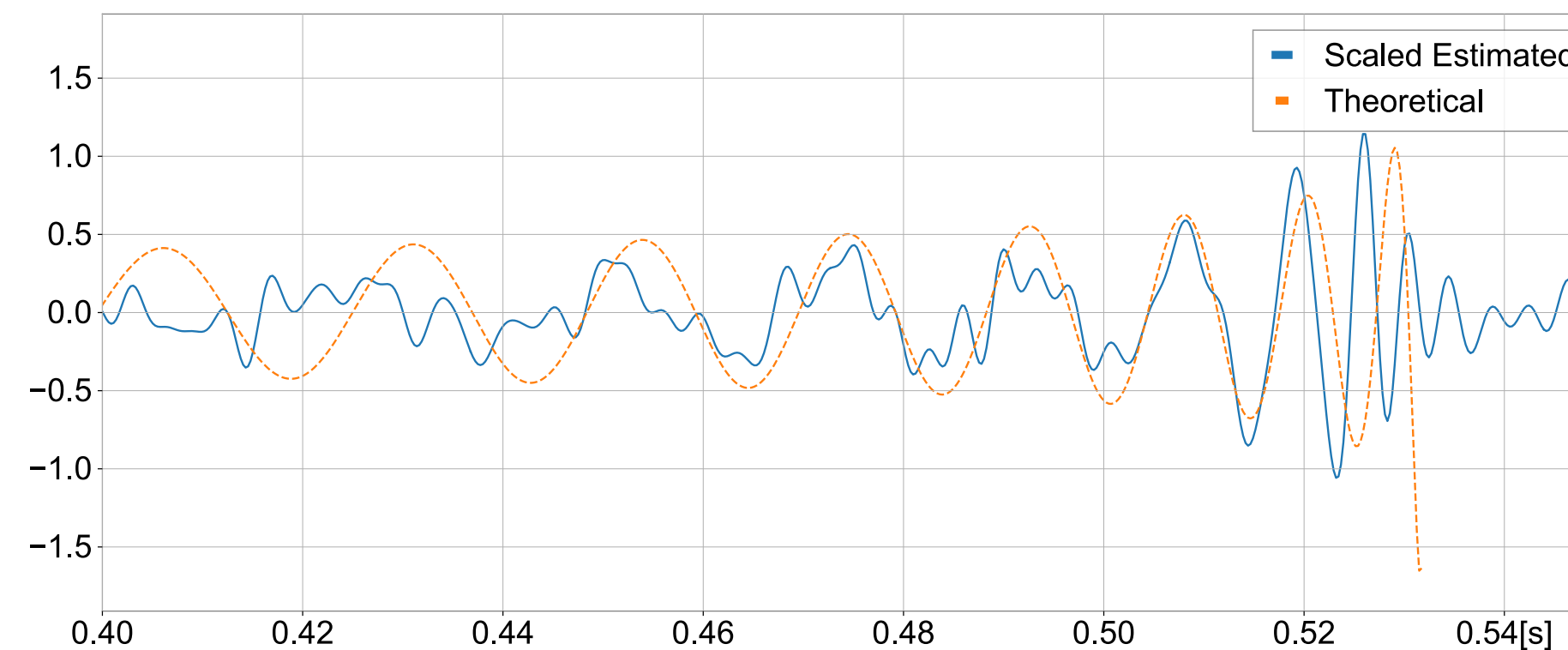
(c) Output of ICA.



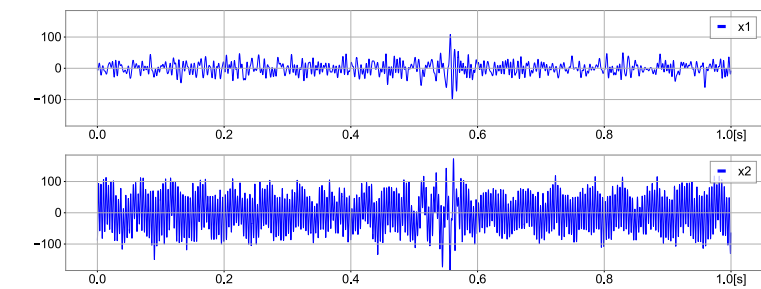
(b) Fourier spectrum of (a).



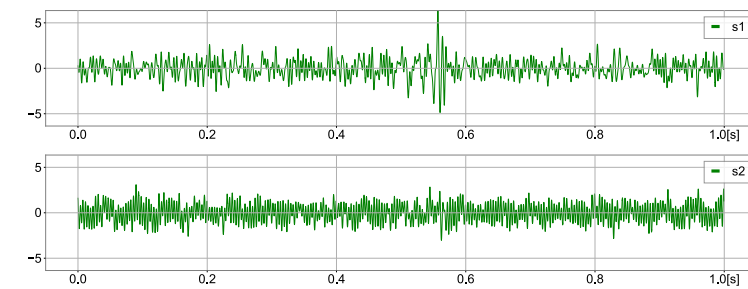
(d) Fourier spectrum of (c).



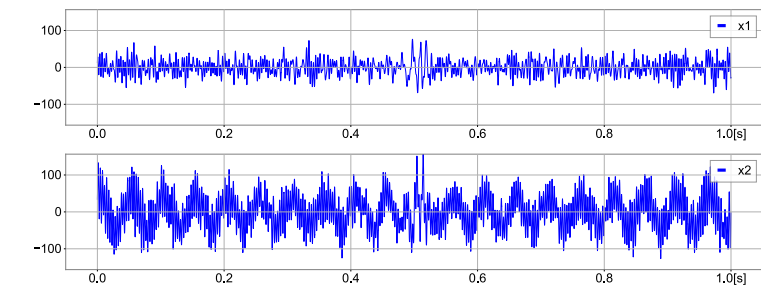
抽出されたGW信号と, inspiral 波形を重ねて, マッチする $M_c(\text{obs})$ を算出
LVK論文で記載されている $M_c(\text{source})$ と, $(1+z)$ のファクターが無矛盾



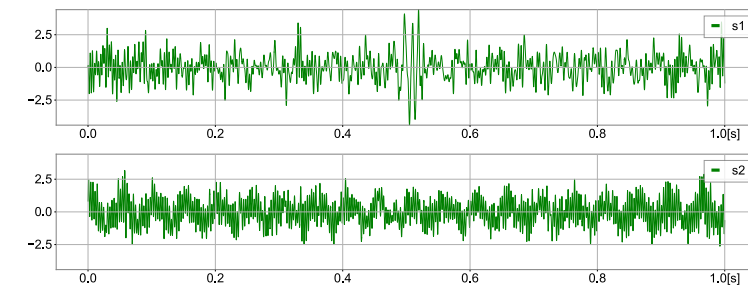
(a1) Input signals of GW190521.074359 with $\Delta t_{HL} = -6.35$ ms. The data x1 and x2 are of Hanford and Livingston data, respectively.



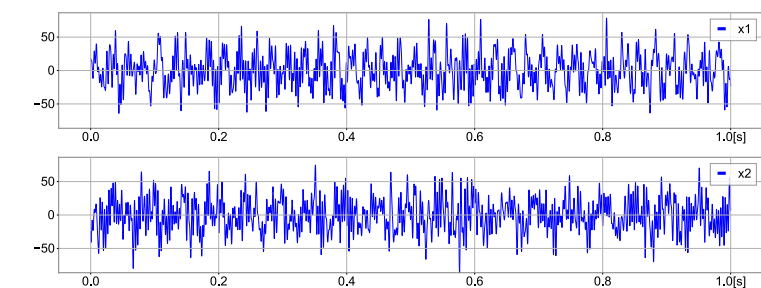
(a2) Output of ICA for GW190521.074359.



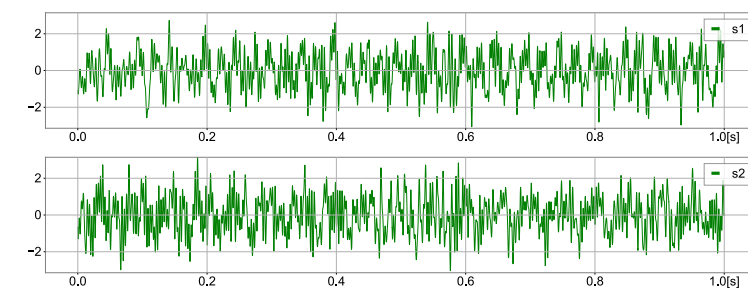
(b1) Input signals of GW191109.010717 with $\Delta t_{HL} = +3.17$ ms. The data x1 and x2 are of Hanford and Livingston data, respectively.



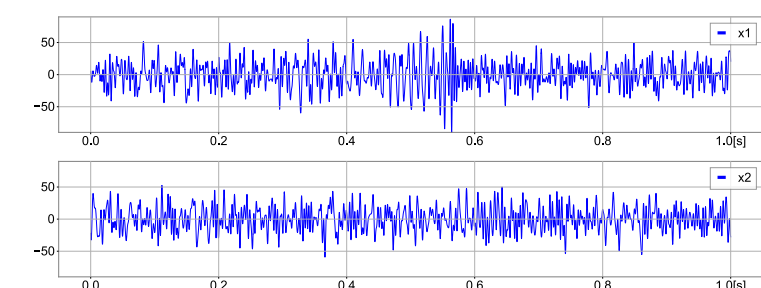
(b2) Output of ICA for GW191109.010717.



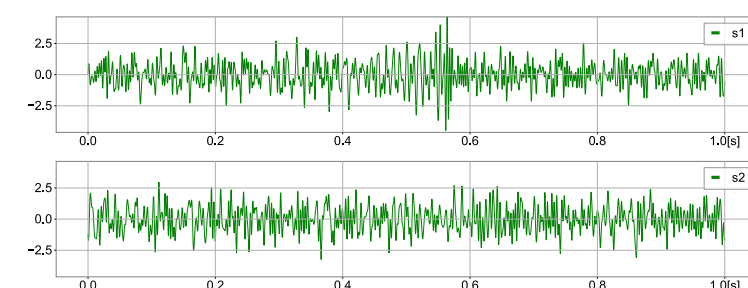
(c1) Input signals of GW191204.171526 with $\Delta t_{HL} = -2.44$ ms. The data x1 and x2 are of Hanford and Livingston data, respectively.



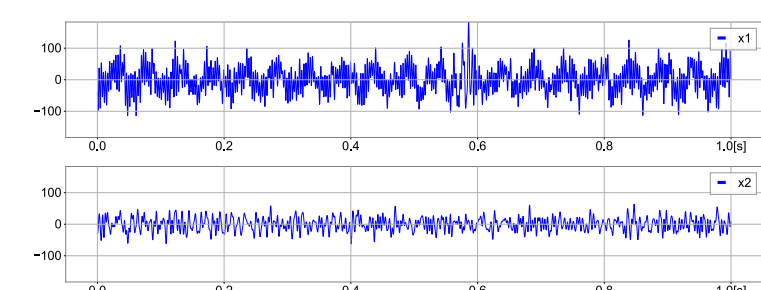
(c2) Output of ICA for GW191204.171526.



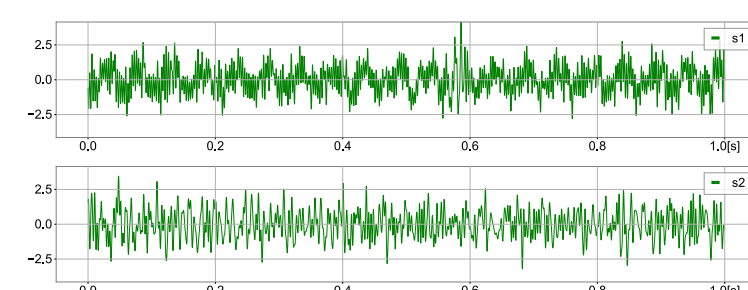
(d1) Input signals of GW191216.213338 with $\Delta t_{HV} = -11.0$ ms. The data x1 and x2 are of Hanford and Virgo data, respectively.



(d2) Output of ICA for GW191216.213338.

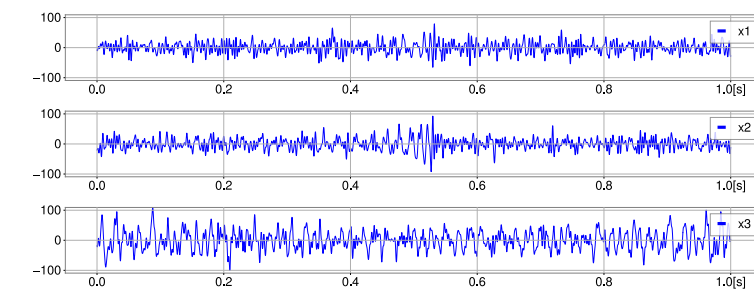


(e1) Input signals of GW200112.155838 with $\Delta t_{LV} = -23.2$ ms. The data x1 and x2 are of Livingston and Virgo data, respectively.

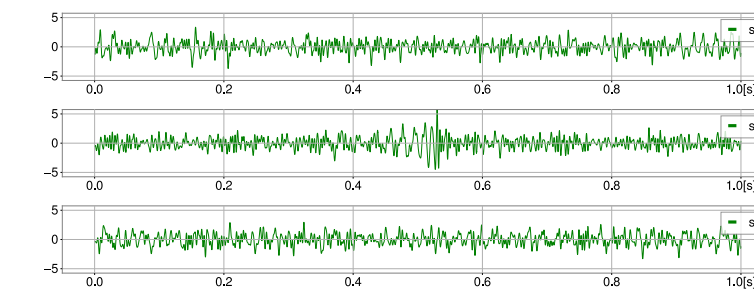


(e2) Output of ICA for GW200112.155838.

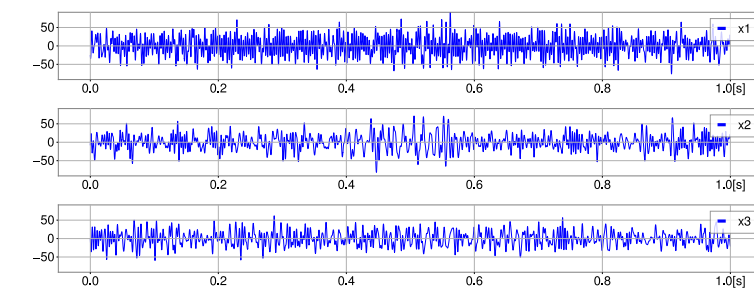
FIG. 7. Input and Output data of ICA analysis.



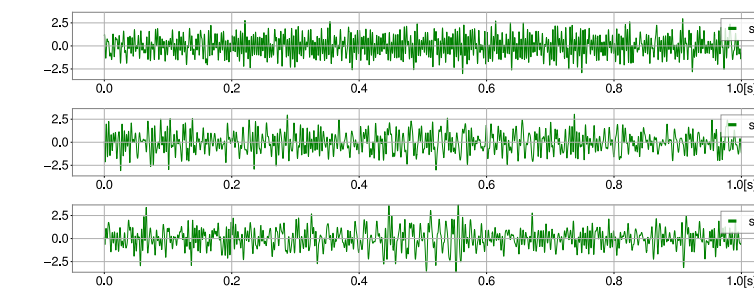
(f1) Input signals of GW170814 with $\Delta t_{HL} = -8.06$ ms and $\Delta t_{HV} = +0.98$ ms. The data x1, x2, and x3 are of Hanford, Livingston, and Virgo, respectively.



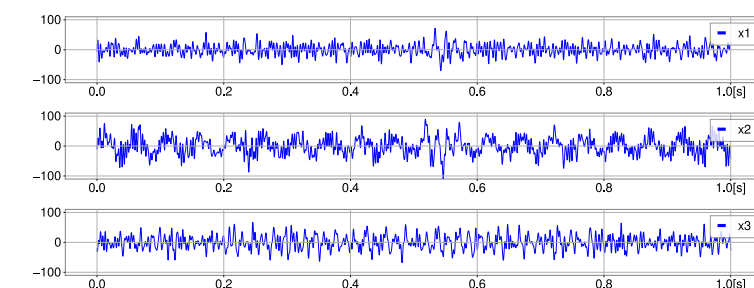
(f2) Output of ICA for GW170814.



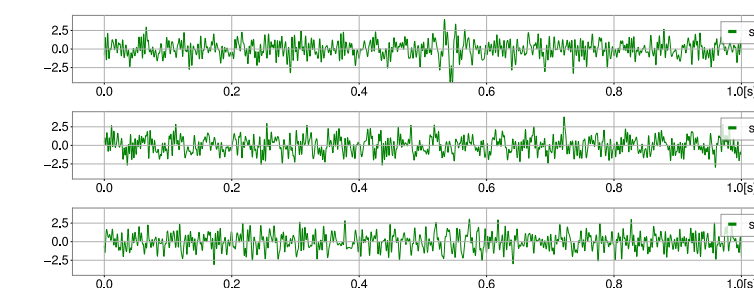
(g1) Input signals of GW190412 with $\Delta t_{HL} = -3.91$ ms and $\Delta t_{HV} = -13.92$ ms. The data x1, x2, and x3 are of Hanford, Livingston, and Virgo, respectively.



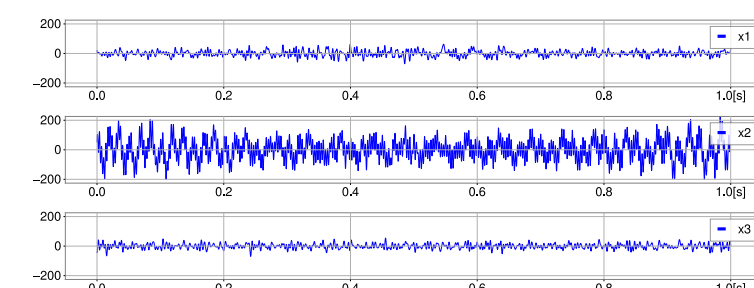
(g2) Output of ICA for GW190412.



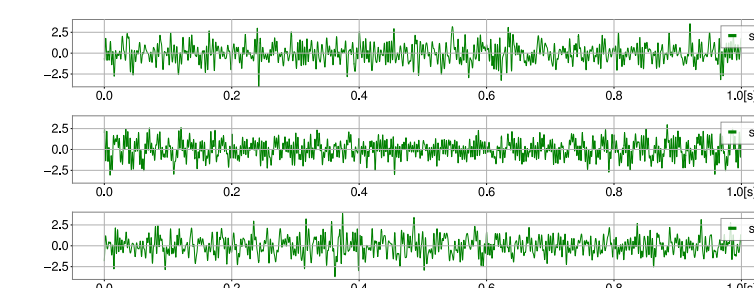
(h1) Input signals of GW190521 with $\Delta t_{HL} = +2.93$ ms and $\Delta t_{HV} = -25.15$ ms. The data x1, x2, and x3 are of Hanford, Livingston, and Virgo, respectively.



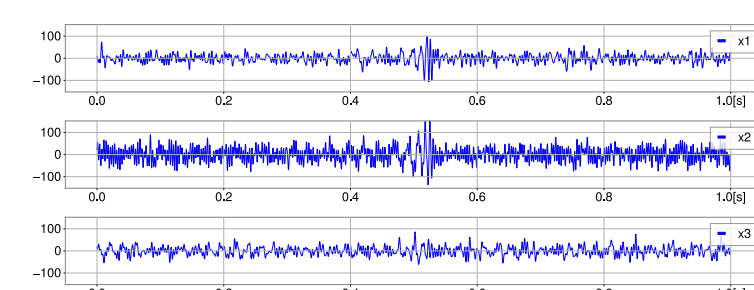
(h2) Output of ICA for GW190521.



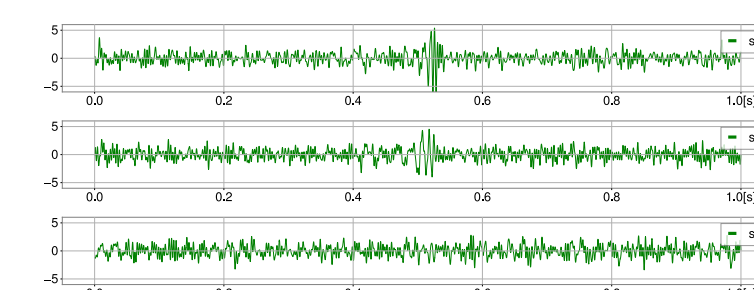
(i1) Input signals of GW190814 with $\Delta t_{HL} = +2.20$ ms and $\Delta t_{HV} = +21.24$ ms. The data x1, x2, and x3 are of Hanford, Livingston, and Virgo, respectively.



(i2) Output of ICA for GW190814.

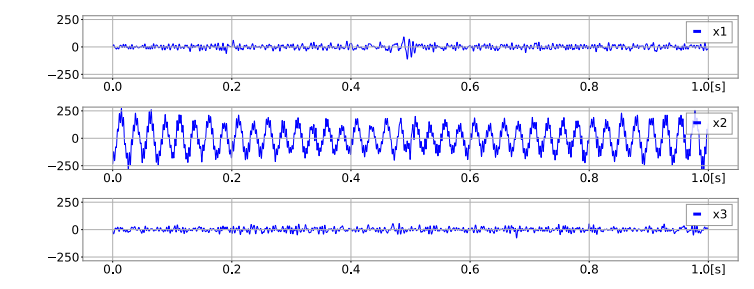


(j1) Input signals of GW200129.065458 with $\Delta t_{HL} = +3.42$ ms and $\Delta t_{HV} = -18.31$ ms. The data x1, x2, and x3 are of Hanford, Livingston, and Virgo, respectively.

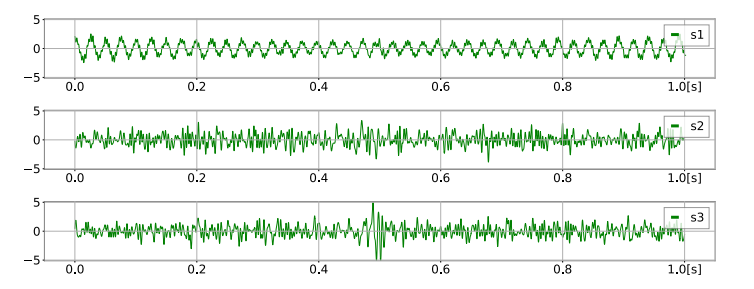


(j2) Output of ICA for GW200129.065458.

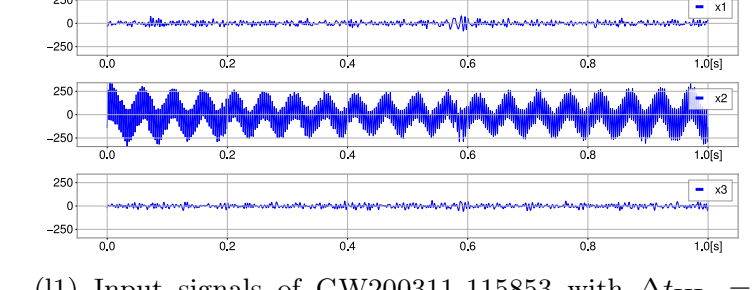
FIG. 7. Input and Output data of ICA analysis (cont.)



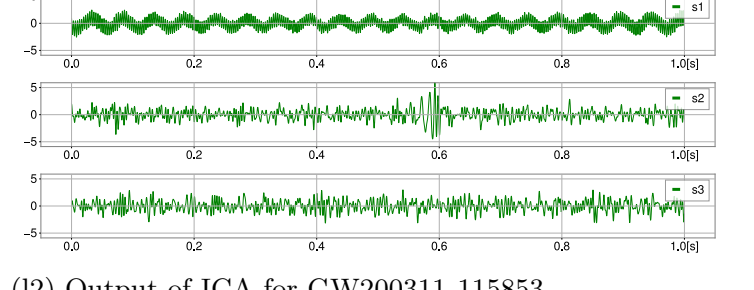
(k1) Input signals of GW200224.222234 with $\Delta t_{HL} = -3.66$ ms and $\Delta t_{HV} = -9.28$ ms. The data x1, x2, and x3 are of Hanford, Livingston, and Virgo, respectively.



(k2) Output of ICA for GW200224.222234.



(l1) Input signals of GW200311.115853 with $\Delta t_{HL} = -3.66$ ms and $\Delta t_{HV} = -27.10$ ms. The data x1, x2, and x3 are of Hanford, Livingston, and Virgo, respectively.



(l2) Output of ICA for GW200311.115853.

FIG. 7. Input and Output data of ICA analysis (cont.)

TABLE III. Results of the wave extractions by ICA for large SNR events in O1-O3. The column obs shows which detector (Hanford/Livingston/Virgo) observed. SNR is the network signal-to-noise ratio (centered value) which is announced in GWOSC (<https://gwosc.org>). Δt_{HL} is the time shift between Hanford data and Livingston data, $t_L - t_H$, in ms when ICA shows the best separation of the signal. \mathcal{A} is the ratio of extracted signal to the other noise(s) evaluated by eq. (10). \mathcal{R} is the residuals of the extracted waveform and estimated inspiral waveform, (11), between $[t_c - 0.15 \text{ ms}, t_c]$. See table IV for comparisons of chirp-mass and red-shift.

event	obs	SNR	Δt_{HL} (ms)	Δt_{HV} (ms)	Δt_{LV} (ms)	\mathcal{A}	$\mathcal{R}/10^{-12}$	ref.
GW150914	HL	26.0	$-7.32 \pm_{1.5}^{1.5}$	—	—	4.19	5.88	Fig.4
GW190521_074359	HL	32.8	$-6.35 \pm_{0.49}^{0.98}$	—	—	1.83	10.3	Fig.7(a)
GW191109_010717	HL	47.5	$3.17 \pm_{0.73}^{0.98}$	—	—	3.40	18.4	Fig.7(b)
GW191204_171526	HL	8.55	$-2.44 \pm_{0.73}^{0.49}$	—	—	2.07	3.27	Fig.7(c)
GW191216_213338	HV	8.33	—	$-11.0 \pm_{0.73}^{1.5}$	—	3.08	2.09	Fig.7(d)
GW200112_155838	LV	27.4	—	—	$-23.2 \pm_{0.24}^{0.49}$	2.43	10.5	Fig.7(e)
GW170814	HLV	24.1	$-8.06 \pm_{0.98}^{0.49}$	$0.98 \pm_{0.24}^{2.4}$	—	3.54	5.07	Fig.7(f)
GW190412	HLV	13.3	$-3.91 \pm_{0.24}^{0.24}$	$-13.92 \pm_{0.49}^{0.98}$	—	2.21	4.40	Fig.7(g)
GW190521	HLV	63.3	$2.93 \pm_{1.2}^{0.49}$	$-25.15 \pm_{1.7}^{0.49}$	—	2.85	31.8	Fig.7(h)
GW190814	HLV	6.11	$2.20 \pm_{0.24}^{0.49}$	$21.24 \pm_{0.24}^{0.73}$	—	2.00	1.65	Fig.7(i)
GW200129_065458	HLV	27.2	$3.42 \pm_{0.24}^{0.98}$	$-18.31 \pm_{0.24}^{0.24}$	—	3.96	11.3	Fig.7(j)
GW200224_222234	HLV	31.1	$-3.66 \pm_{0.24}^{2.7}$	$-9.28 \pm_{0.98}^{0.24}$	—	3.28	13.4	Fig.7(k)
GW200311_115853	HLV	26.6	$-3.66 \pm_{1.2}^{0.73}$	$-27.10 \pm_{2.2}^{2.2}$	—	3.17	4.34	Fig.7(l)

SNRが高いものと, GW190521

ICAがGW信号を他と分離したときの
背景ノイズとの比 あまり変わらない

抽出されたGW信号と, inspiral 波形を
重ねた時の残差 SNRが高いと残差小さい

TABLE IV. Comparisons of chirp mass, M_c^{source} , shown in GWOSC and the one obtained by ICA, M_c^{obs} from the best fit inspiral-wave model. The difference can be regard as redshift factor $(1 + z_{\text{ICA}})$. The redshift factor in GWOSC, z , is also shown.

event	obs	SNR	GWOSC		ICA		ref.
			$M_c^{\text{source}}/M_\odot$	z	M_c^{obs}/M_\odot	z_{ICA}	
GW150914	HL	26.0	$28.6^{+1.7}_{-1.5}$	$0.09^{+0.03}_{-0.03}$	30.8	$0.077^{+0.06}_{-0.06}$	Fig.4
GW190521_074359	HL	25.9	$32.8^{+3.2}_{-2.8}$	$0.21^{+0.10}_{-0.10}$	36.4	$0.11^{+0.10}_{-0.10}$	Fig.7(a)
GW191109_010717	HL	17.3	$47.5^{+9.6}_{-7.5}$	$0.25^{+0.18}_{-0.12}$	53.7	$0.13^{+0.22}_{-0.19}$	Fig.7(b)
GW191204_171526	HL	17.5	$8.56^{+0.41}_{-0.28}$	$0.34^{+0.25}_{-0.18}$	11.1	$0.29^{+0.04}_{-0.06}$	Fig.7(c)
GW191216_213338	HV	18.6	$8.33^{+0.22}_{-0.19}$	$0.07^{+0.02}_{-0.03}$	9.00	$0.08^{+0.03}_{-0.03}$	Fig.7(d)
GW200112_155838	LV	19.8	$27.4^{+2.6}_{-2.1}$	$0.24^{+0.07}_{-0.08}$	32.7	$0.19^{+0.10}_{-0.10}$	Fig.7(e)
GW170814	HLV	17.7	$24.1^{+1.4}_{-1.1}$	$0.12^{+0.03}_{-0.04}$	26.0	$0.08^{+0.05}_{-0.06}$	Fig.7(f)
GW190412	HLV	19.8	$13.3^{+0.5}_{-0.5}$	$0.15^{+0.04}_{-0.04}$	14.8	$0.11^{+0.04}_{-0.04}$	Fig.7(g)
GW190521	HLV	14.3	$63.3^{+19.6}_{-14.6}$	$0.56^{+0.36}_{-0.27}$	81.7	$0.29^{+0.39}_{-0.30}$	Fig.7(h)
GW190814	HLV	25.3	$6.11^{+0.06}_{-0.05}$	$0.05^{+0.01}_{-0.01}$	6.35	$0.04^{+0.01}_{-0.01}$	Fig.7(i)
GW200129_065458	HLV	26.8	$27.2^{+2.1}_{-2.3}$	$0.18^{+0.05}_{-0.07}$	30.6	$0.13^{+0.10}_{-0.08}$	Fig.7(j)
GW200224_222234	HLV	20.0	$31.1^{+3.3}_{-2.7}$	$0.32^{+0.08}_{-0.11}$	37.6	$0.21^{+0.11}_{-0.12}$	Fig.7(k)
GW200311_115853	HLV	17.8	$26.6^{+2.4}_{-2.0}$	$0.23^{+0.05}_{-0.07}$	31.0	$0.17^{+0.09}_{-0.10}$	Fig.7(l)

抽出されたGW信号に合致するインスパイラル波形の $M_c(\text{obs})$ を算出
 LVK論文の $M_c(\text{source})$ と比較して $(1+z)$ を算出
 すべてのイベントで無矛盾

独立成分分析を用いた重力波抽出方法の提案

[arXiv:2503.14179](https://arxiv.org/abs/2503.14179)

Gravitational-wave Extraction using Independent Component Analysis

下村りか, 田部優一, 真貝寿明 (大阪工大情報科学部)

Rika Shimomura, Yuuichi Tabe, Hisaaki Shinkai (OIT)

まとめ

- テンプレートを用いずに、重力波の波形を取り出す新たな手法を提案した
- Injection testにより、**干渉計の実ノイズでも、SNR>15** で有効
- O3までの実イベント12例に応用
 - 波形を抽出でき、 $M_c(1+z)$ も GWTC3と無矛盾
 - **すべてのイベントでGW波形を無矛盾に抽出できたといえる**
 - 干渉計への重力波到着時刻の誤差を小さくできる例あり
 - **sky localizationの精度向上へ使える**

利点

- 計算も軽い. Laptop PCで可能(3干渉計なら数時間)
- テンプレート不要なので, 例えば,
 - 一般相対性理論の検証
 - 未知の重力波の発見

課題

- ICAで分離される結果は, 振幅の大きさ情報をもたない.
- ICAで分離される結果は, 位相反転している可能性がある.

コメント

先の2023年3月の物理学会で報告したAR(自己回帰モデル)もテンプレートなしで波形抽出できた. いろいろな重力波抽出方法の開発ができつつあり, 比較検証ができるようになる. サイエンスが確かになって, 楽しい.

科研費に謝辞 This work was supported by JSPS KAKENHI Grants No. 24K07029 and 18K03630.